

## Chapter 7

# Geology and Exploration Progress at the Resolution Porphyry Cu-Mo Deposit, Arizona

CARL HEHNKE,<sup>1</sup> GEOFF BALLANTYNE,<sup>2,1</sup> HAMISH MARTIN,<sup>1</sup> WILLIAM HART,<sup>1</sup> ADAM SCHWARZ,<sup>3</sup> AND HOLLY STEIN<sup>4</sup>

<sup>1</sup>Resolution Copper Mining, 102 Magma Heights, Superior, Arizona 85273

<sup>2</sup>Rio Tinto Copper Development, 4700 Daybreak Parkway, South Jordan, Utah 84095

<sup>3</sup>Northparkes Mines, Northparkes Lane, Goonumbla, New South Wales 2870, Australia

<sup>4</sup>AIRIE Program, Colorado State University, Fort Collins, Colorado 80523-1482

### Abstract

In 1995, the Magma Copper Company discovered a porphyry copper deposit beneath thick postmineral cover 2 km south of the historic Magma mine in Superior, Arizona. Since that time drilling has delineated a large, high-grade, hypogene copper-molybdenum deposit, now named the Resolution deposit, with an Inferred Resource of 1,624 million metric tons (Mt) at 1.47% Cu and 0.037% Mo.

The Resolution deposit is hosted by Proterozoic and Paleozoic quartzite and carbonate units, Proterozoic diabase sills, and Cretaceous sandstone, volcanoclastic rocks, and tuff. Minor Cretaceous to Tertiary hypabyssal intrusions and heterolithic breccia bodies cut this Proterozoic-to-Mesozoic section. The mineralized rocks are concealed beneath an eastward-thickening wedge of Oligo-Miocene Whitetail Conglomerate, which in turn is largely covered by 18.6 Ma welded tuff.

The porphyry copper deposit at Resolution is centrally located within a fault-bounded block with plan dimensions of  $\sim 3 \times 3$  km. The fault-bounded block first developed as a horst, which led to local erosion of Paleozoic strata but was later inverted as a graben, which preserves  $\sim 1$  km of Cretaceous strata not otherwise present in the Superior area. Within the graben, basal quartz-rich sedimentary rocks containing  $\sim 97$  Ma zircons are overlain by a  $\sim 74$  Ma andesitic sequence that was probably derived from outside the graben. Younger units consist mostly of quartz-rich tuffs, whose petrographic similarity and U-Pb ages suggest they are extrusive equivalents of  $\sim 69$  to  $\sim 64$  Ma hypabyssal intrusions present at depth within the graben. Crustal extension and tilting across multiple, large Tertiary normal faults since the onset of Whitetail Conglomerate deposition has rotated the deposit approximately  $25^\circ$  to the east northeast.

Copper mineralization at Resolution defines a structurally intact, dome-shaped shell up to 600 m thick, the upper boundary of which is overlapped by an unusually strong pyrite halo containing 7 to  $>14$  wt % pyrite. The deposit shows strong alteration and mineralization zoning and strong telescoping of alteration assemblages. Early potassic alteration, associated with dominantly chalcopyrite-rich mineralization, gives way outward to an epidote-bearing propylitic zone. Strong quartz-sericite alteration largely overprints the upper portion of the potassic zone and is associated with chalcopyrite, bornite, chalcocite, and pyrite mineralization. Structurally controlled advanced argillic alteration, consisting of kaolinite, dickite, topaz, alunite, pyrophyllite, and zunyite overprints the quartz-sericite zone and is associated with pyrite as well as hypogene bornite, chalcocite, and digenite, which have substantially replaced earlier chalcopyrite. Molybdenite occurs in quartz veins both with and without copper minerals but economic concentrations of copper and molybdenum are spatially coincident.

Re-Os ages for molybdenite range from  $\sim 65$  to  $\sim 64$  Ma, coinciding with the youngest U-Pb age for hypabyssal intrusions. The  $^{40}\text{Ar}/^{39}\text{Ar}$  ages of biotite and sericite range from  $\sim 64$  to  $\sim 62$  Ma and  $^{40}\text{Ar}/^{39}\text{Ar}$  ages for hypogene alunite range from  $\sim 62$  to  $\sim 60$  Ma. Younger,  $\sim 52$  to 49 Ma  $^{40}\text{Ar}/^{39}\text{Ar}$  dates for two hypogene alunite veins, and a  $\sim 51$  Ma Re-Os pyrite date for a massive pyrite-dickite vein, may indicate a later pulse of hydrothermal activity.

A clearly defined causative intrusion has not been identified at Resolution but strong foliation defined by secondary biotite within the host diabase sills mimics the dome-shaped copper shell and is inferred to reflect stress due to emplacement of a cylindrical stock below the deepest drill holes. Unusually high hypogene copper grades reflect the presence of favorable diabase and limestone host rocks, lack of dilution by postmineral dikes, and multiple spatially overlapping mineralizing events, including the deposition of early chalcopyrite, later chalcopyrite-bornite, and still later bornite-chalcocite-digenite assemblages. The high grades may also reflect an unusually long-lived flux of ore fluids channeled through the center of the deposit by permeable breccia zones.

### Introduction

THE RESOLUTION porphyry copper-molybdenum deposit is located beneath a minimum of 1 km of postmineral cover south of the historic Magma mine in the Superior (Pioneer)

mining district, approximately 90 km east of Phoenix, Arizona (Fig. 1). The Magma mine was active until 1996 and over its life produced more than 23 Mt of ore at an average grade of 5% Cu (Hammer, 1989). The surface above the deposit is a rugged plateau at an elevation of 1,200 m located immediately east of a prominent escarpment known as Apache Leap

<sup>†</sup> Corresponding author: e-mail, geoff.ballantyne@riotinto.com



FIG. 1. Location of the Resolution deposit and other porphyry-style deposits in the region.

that overlooks the town of Superior (Fig. 2). The project is owned by Resolution Copper Mining L.L.C. (RCML), which is jointly controlled by Rio Tinto (55%) and BHP Billiton (45%).

Resolution occurs within a well-known province of porphyry copper deposits, including the active Ray mine located 13 km south of Resolution, with production of 95,254 t Cu in 2010 (Grupo Mexico, 2010). Pinto Valley, 14 km to the north-east, was active as recently as 2008 with production of 39,500 t Cu (BHP Billiton, 2009) and is scheduled to restart in late 2012 (BHP Billiton website, 14 February 2012). Currently, the largest porphyry copper deposit in the region is Morenci, located ~175 km to the east with total production plus resource of 6,470 Mt at 0.52% Cu (Singer et al., 2008). By comparison, the present Inferred Resource at Resolution stands at 1,624 Mt of 1.47% Cu and 0.037% Mo (Rio Tinto, 2010).

This paper reviews the exploration history of the Resolution deposit, describes its regional geologic and metallogenic setting, and presents details of the geology, hydrothermal alteration and mineralization of the deposit as currently understood from drilling. Although the descriptions and interpretations are based primarily on in-house work completed by the authors, this paper also draws heavily on both published and

unpublished work (e.g., Hammer, 1972, 1989; Paul and Manske, 1998; Manske and Paul, 2002; Zulliger, 2007).

The discovery in 1995 of this high-grade porphyry copper deposit was unexpected, given its location within a mature porphyry copper province, especially a province that is characterized by typical hypogene copper grades of less than 0.4% Cu (Lowell and Guilbert, 1970). But in hindsight, the potential for a significant porphyry deposit under cover on the plateau above Superior is suggested by the high-grade mineralization in the Magma mine, barely 1 km to the north-north-west, and the large number of easterly trending Cu-Ag-bearing veins along the range front (Figs. 2, 3).

### Discovery and Resource Delineation

#### *Magma mine discovery and development*

Discovery of the Resolution deposit is the latest chapter in a rich history of exploration, discovery, and mining near Superior. An 86-year period of almost continuous operation began when the Silver Queen, originally staked in 1875 (Chappell, 1973), was reopened as the Magma mine in 1910. The short, irregular, supergene chalcocite ore shoots originally mined for native silver were found to change downward

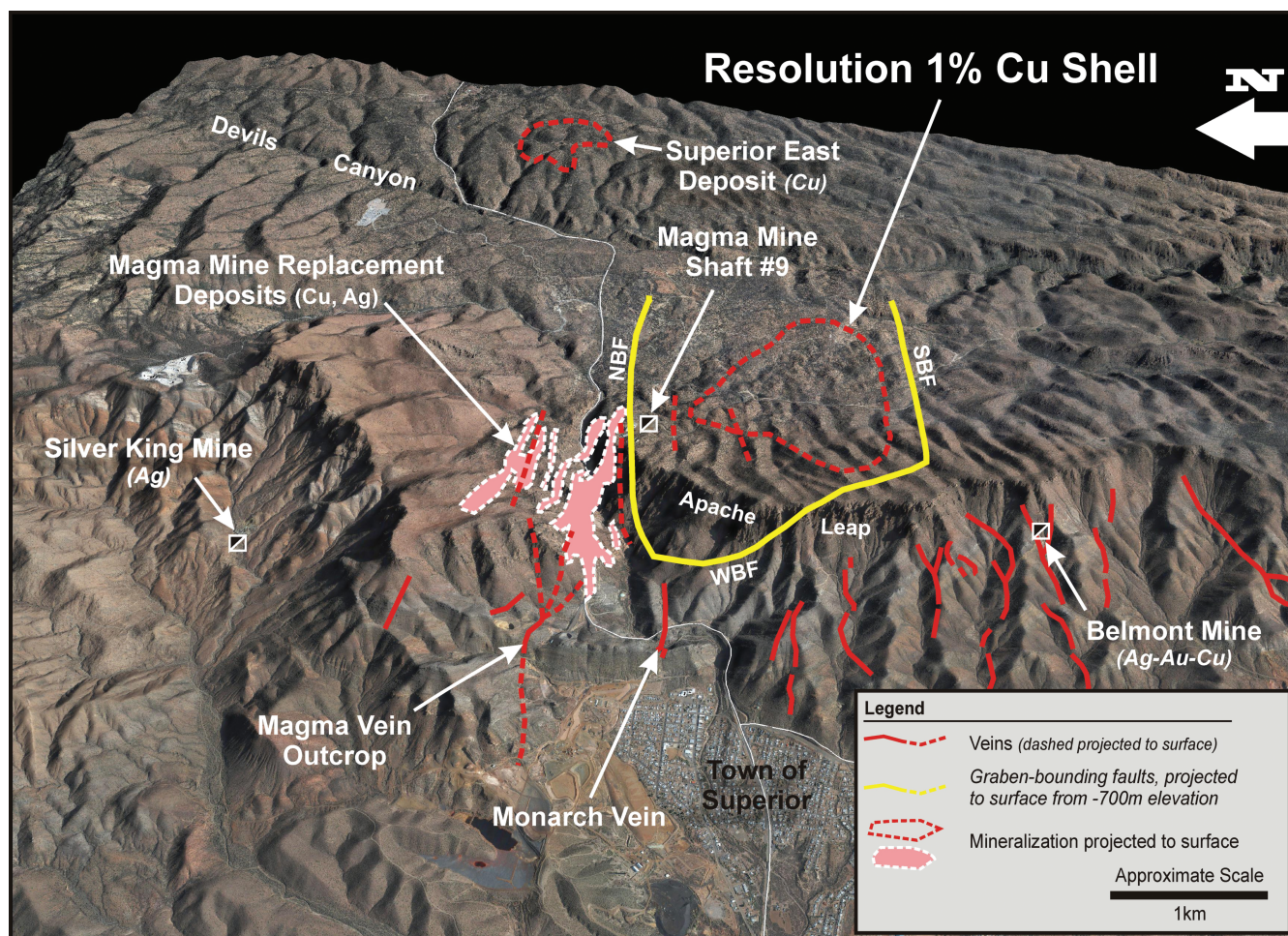


FIG. 2. Oblique view looking east, showing Resolution deposit and graben in relationship to the Magma mine to the north, and numerous veins to the west along the base of Apache Leap. Base map is satellite imagery draped on topography. The Superior East deposit is located approximately 9 km east-northeast of Superior. Scale shown is approximate in this oblique view. Abbreviations: NBF = North Boundary fault, SBF = South Boundary fault, WBF = West Boundary fault.

to more continuous hypogene chalcocite-bornite mineralization with depth (Ransome, 1912), and significant copper production began.

The Magma and related veins, which were followed along strike and mined as deep as 1,500 m below surface, constituted the principal source of ore through 1954. In 1948 manto-style copper mineralization, in what was later designated as the A-bed of the Devonian Martin Formation, was discovered while drilling for vein offsets. After delineation of this relatively shallow replacement ore (Fig. 4), production along the veins was gradually phased out and there was no production from the Magma vein after 1966 (D.F. Hammer, pers. commun., 2011). Development of the A-bed manto deposit initiated exploration that eventually discovered at least six productive horizons in the Martin, Mississippian Escabrosa, and the basal part of the Pennsylvanian Naco Formations. These exploration efforts also resulted in discovery of a previously unknown graben after underground workings crossed what was to be termed the North Boundary fault (Figs. 2–4), thus setting in motion almost 30 years of exploration efforts that would eventually result in discovery of the Resolution deposit.

#### Resolution discovery

The E-W-trending North Boundary fault (Fig. 3), which is locally mineralized and acted as a conduit for ore fluids to the mantos, juxtaposes the Paleozoic section to the north with a sequence of Cretaceous sedimentary and volcanic rocks (designated Kvs) to the south (Fig. 4). By 1966, Magma mine geologists had also identified the West Boundary fault, which delineates the western limit of Kvs. Although these two faults were estimated to have at least 750 m of displacement (Hammer, 1967), the relatively small displacement “N-S 5W” fault identified in workings to the north was determined to be a northern continuation of the West Boundary fault. The Monarch vein cropping out on the range front was identified as the westward continuation of the North Boundary fault. Hammer (1967) postulated a southern boundary fault along the eastern projection of the Belmont vein (Fig. 2), analogous to the Monarch vein and its relationship to the North Boundary fault, and suggested potential for high-grade mineralization along this southern boundary.

In a report a few years later, Hammer (1972, p. 41) suggested the “...possibility that mineralized intrusive rocks underlie

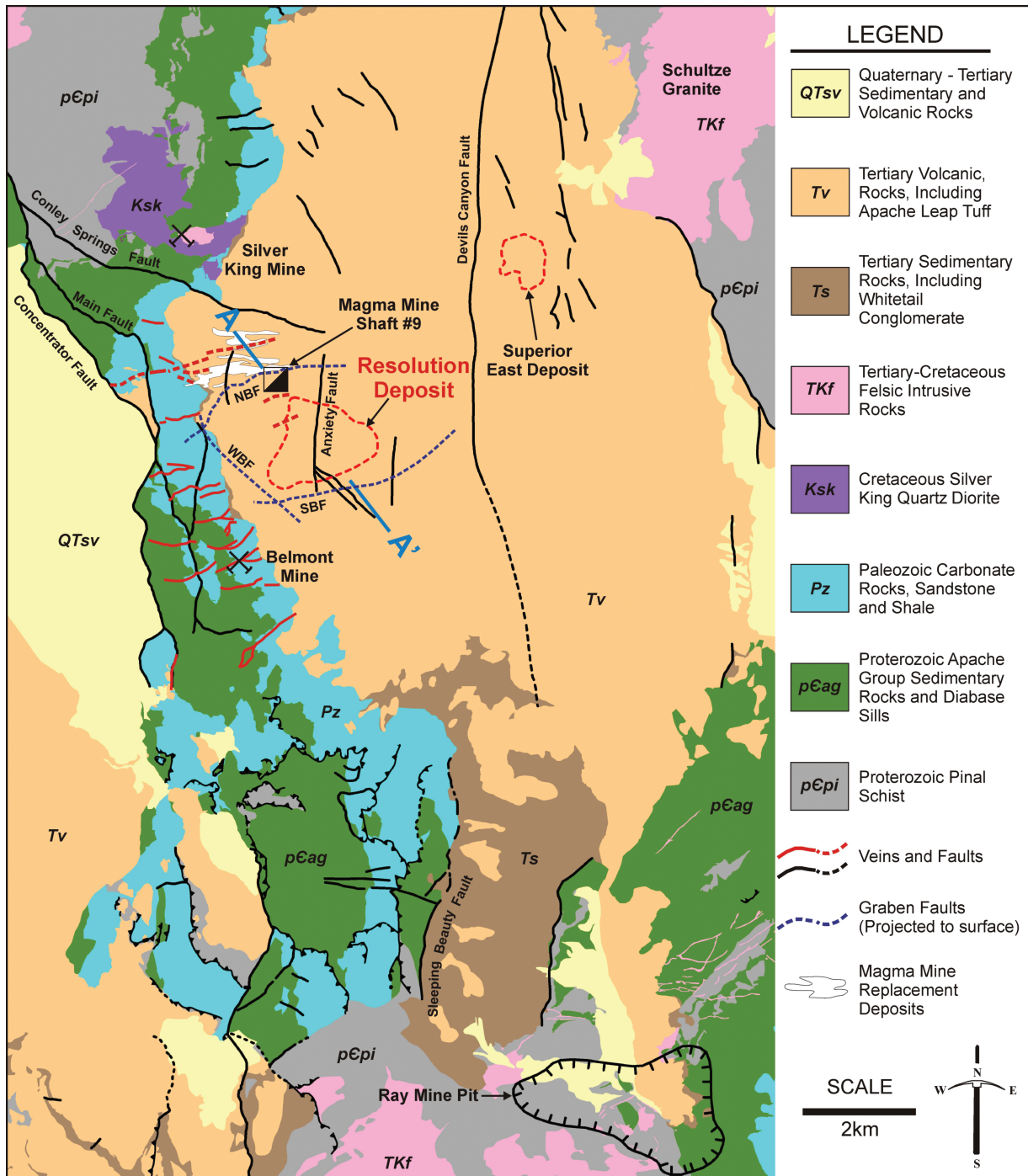


FIG. 3. Geology of the Resolution, Superior East, and Ray area, modified from Peterson (1963), Peterson (1969), Cornwall et al. (1971), and Creasey et al. (1983). For abbreviations, see Figure 2 caption.

the volcanic plateau east of the Belmont mine.” Despite recognition of this porphyry target, and a later paper suggesting an association of the magma veins and mantos with an as-yet undiscovered porphyry system (Einaudi, 1982), the focus of exploration for magma copper through the mid-1990s continued to be discovery of additional vein and replacement deposits to augment the reserves of the Magma mine (Paul and Manske, 1998). Importantly, identification of the graben and

recognition of its mineral potential resulted in acquisition of land needed to secure the eventual discovery at Resolution (Hammer, 1967).

Beginning in 1973 Magma Copper initiated surface drilling to locate the South Boundary fault by targeting photo lineaments east of the Belmont mine, but it was not until 1991 that Magma’s geologists were successful in crossing the fault and intersecting narrow chalcopyrite ± bornite veins (Manske and

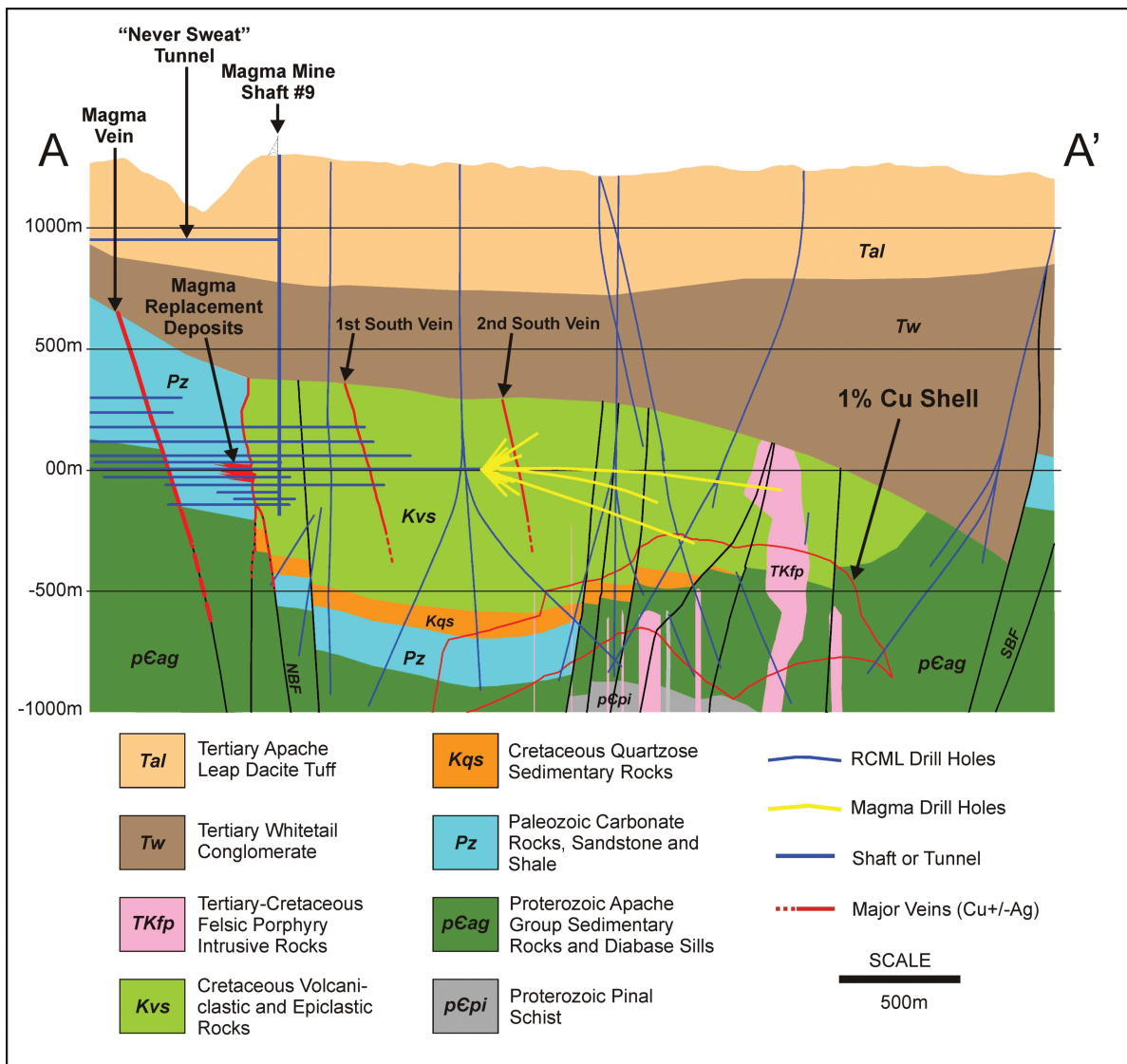


FIG. 4. Cross section of geology, looking northeast through the Magma shaft 9 and Resolution deposit. Abbreviations: RCML = Resolution Copper Mining L.L.C.; see also Figure 2 caption.

Paul, 2002). These results, along with discovery in the 1970s of the First South and Second South veins located south of the Magma shaft 9 (Fig. 4), confirmed the prospectivity of the entire graben and justified drilling hole S27E, an 1,100-m-long horizontal core hole in 1994; the hole was drilled from the southernmost workings of the Magma mine at about sea level (Fig. 4). Hole S27E intersected 460 m of quartz-sericite-pyrite-altered Cretaceous rocks that assayed 0.56% Cu, marking the discovery of the Resolution porphyry copper deposit (Paul and Manske, 1998; Manske and Paul, 2002).

Drill hole S27H, an inclined underground hole drilled a year later to follow up on S27E, bottomed in hydrothermal breccia with relict potassic alteration and stockwork chalcopyrite-molybdenite veins that assayed 1.94% Cu and 0.037% Mo over 43 m. Two additional underground holes intersected strong porphyry-style mineralization, and in 1998 two surface holes were completed. One of the surface holes, MB-20A, intersected 306 m at 1.75% Cu and 0.029% Mo, the

best intercept to that date. Despite this high-grade but deep discovery, a decision was made to pull out the water pumps and close the Magma mine in 1998. BHP entered into an exploration agreement with Rio Tinto's North American subsidiary Kennecott Exploration in April 2001.

#### Initial Kennecott drilling

Kennecott's drilling program, initiated in July 2001, was designed to test the deposit to a depth of ~2 km. To improve the odds of completing core holes to these depths, large mudrotary rigs were deployed to drill and case mother holes to ~1-km depth. After completing vertical core holes beneath each mother hole, directional drilling techniques were used to drill two to four daughter holes from each precollar. Seventeen core holes completed by January 2003, established the continuity of strong mineralization in an area at least 1 km in diameter. The best mineralized interval was 587 m and averaged 2.03% Cu and 0.036% Mo.

It was recognized during this initial phase of drilling that the upper boundary of the deposit is defined by an abrupt change from spotty mineralization averaging less than 0.5% Cu to consistent mineralization assaying >1% Cu where chemically reactive host rocks are present. Locally, a lower boundary of >1% Cu mineralization was also defined but the grade change at this boundary is more gradual. The zone enclosed by the upper and lower boundaries of >1% Cu mineralization is referred to as the "1% Cu Shell" in this paper. The outline of the 1% Cu Shell is shown in several of the maps and cross sections.

#### *Delineation drilling*

Delineation drilling commenced following completion of Order-of-Magnitude studies in 2002 and 2005, which evaluated a block-cave mining operation. As of January 2012, 76 core holes had been completed from 16 sites. Much of the deposit has now been drilled at a spacing of approximately 200 m. The current focus is to complete a nominal 150-m-spaced grid within the area expected to be mined in the first 10 years of production. Geostatistical analysis suggests that a 150-m drill spacing will allow that portion of the deposit to be upgraded to Indicated Resource status.

Currently the project is in prefeasibility stage. Construction of an 8.5-m-diameter shaft to a depth of 2 km is in progress and underground drifting at the planned production level is scheduled as part of the feasibility study. This work is designed to evaluate the geological and geotechnical models generated from surface drilling and to demonstrate the ability to safely and efficiently advance the mine headings required to bring the deposit into production.

### Regional and District Geologic Setting

#### *Regional geology*

The Resolution deposit lies within a cluster of porphyry copper deposits that is centered in east-central Arizona but extends into New Mexico and northern Mexico (Keith and Swan, 1995; Fig. 1). This porphyry copper cluster occurs in an area of complex cratonic architecture and is inferred to have overlain the subducting Farallón plate from Late Cretaceous to the Eocene. The regional geology and tectonics have been studied extensively, e.g., Titley (1982), Keith and Swan (1995), and Leveille and Stegen (2012).

#### *District geology*

The geology in the vicinity of the Resolution deposit is shown in Figure 3. The local geologic column, from oldest to youngest lithologic unit, is as follows:

*Pinal Schist:* The oldest unit, the Pinal Schist, is greenschist-facies schist developed from Paleoproterozoic turbidites (Keep, 1996). Pinal Schist hosts mineralization at the Ray mine (Phillips et al., 1974) and at Superior East (Sell, 1995). However, at Resolution the schist has been intersected in only a few of the deepest drill holes at depths below the base of the 1% Cu Shell.

*Apache Group and Troy Quartzite:* The Apache Group, a >500-m-thick sedimentary sequence of Mesoproterozoic age, disconformably overlies the Pinal Schist (Wrucke, 1989) and comprises the Pioneer Shale, Dripping Spring Quartzite,

Mescal Limestone, and basalt flows. The Troy Quartzite overlies the Apache Group in the Superior district.

*Diabase sills:* The Apache Group and Troy Quartzite are dilated by regionally extensive diabase sills dated at 1.1 Ga, which inflate the original thickness of the older Proterozoic section by up to 100% (Wrucke, 1989). The diabase sills are important host rocks for copper mineralization at both Ray (Phillips et al., 1974) and Resolution.

*Paleozoic sedimentary rocks:* The Cambrian Bolsa Quartzite and a conformable sequence composed of the Devonian Martin Formation, Mississippian Escabrosa Limestone, and Pennsylvanian-Permian Naco Group carbonate rocks overlie the Apache Group and crop out extensively west of Resolution. The carbonate units host replacement mineralization in the Magma mine (Hammer and Peterson, 1968; Paul and Knight, 1995) but are partially removed by erosion at Resolution and absent at Superior East and Ray.

*Cretaceous sedimentary and volcanic rocks:* A 1-km-thick sequence of sandstone, graywacke and volcanoclastic rocks, including minor tuff horizons, is preserved in a graben in the immediate area of the Resolution deposit (Manske and Paul, 2002; Fig. 4). This sequence is not exposed in the area of Figure 3, but when it was encountered in the Magma mine workings during the 1960s, the mine staff recognized that the lithologies were similar to Cretaceous rocks exposed in the Reed basin near the Christmas mine (Hammer, 1967). This sequence hosts the shallowest part of the Resolution deposit and is described in detail below.

*Laramide (Late Cretaceous-Early Tertiary) intrusions:* Several large Laramide plutonic bodies crop out within 20 km of Resolution. Principal among these are the Schultze Granite (Stavast, 2006); the Tortilla quartz diorite, Teapot Mountain Porphyry, and Granite Mountain Porphyry in the Ray area (Cornwall et al., 1971; Phillips et al., 1974); and the Silver King quartz diorite north of Superior (Peterson, 1969). Minor Laramide intrusions are known from drill holes at Superior East (Sell, 1995) and at Resolution, as described in the following sections.

*Tertiary sedimentary and volcanic rocks:* The Oligo-Miocene Whitetail Conglomerate, a coarse basin fill comprised of eroded fragments of all the rock types described above, occupies a basin that extends from Superior east to Globe (Sell, 1995, fig. 3). The conglomerate, which attains a thickness of >1.5 km in a half graben bounded to the east by the Devils Canyon fault, contains abundant exotic copper as native copper and cuprite. The Whitetail Conglomerate is largely covered by the 500-m-thick Miocene Apache Leap dacitic tuff, which forms the prominent volcanic plateau that covers the Resolution and Superior East deposits and extends south to Ray.

#### *Structural geology*

An old, NE- to E-NE-trending structural fabric in east-central Arizona is indicated by the dominant foliation in Pinal Schist, the northeast trend of the 1.4 Ga Ruin Granite (Creasey, 1980), and regional scale magnetic anomalies (U.S. Geological Survey, 2002). This E-NE trend is also indicated by the distribution and elongation of Laramide intrusions, the distribution of mineral deposits, and the orientation of veins and dikes, as reported by Heidrick and Titley (1982). In the

Superior area, the Magma vein and related veins, the First South and Second South veins, and most of the veins below Apache Leap show an E-W to E-NE trend.

Faulting typical of Laramide-aged deformation is well documented in the region. Thrust faults are mapped in Telegraph Canyon, southwest of Superior, and near Ray (Richard and Spencer, 1998), and Laramide-aged reverse movement is described along the N-NE-trending Sleeping Beauty fault north of Ray (Keith, 1986). The Elm Canyon Overthrust (Short et al., 1943) is located at the base of Apache Leap.

Extending north and south of the town of Superior is a 25-km-long belt of well-exposed, early Proterozoic through Paleozoic-aged strata, which dip 25° to 45° E. Drilling confirms that these strata continue at depth under the eastward-thickening Whitetail Conglomerate. Oriented drill core demonstrates that bedding attitudes in Whitetail Conglomerate increase progressively downsection from almost flat near the base of the Apache Leap tuff to ~25° to the east-northeast near its base. East of the Devils Canyon fault, a 500-m-thick section of Whitetail Conglomerate is deposited directly on Pinal Schist. Stratigraphic relationships suggest that the Devils Canyon and related faults accommodated at least 1,800 m of down-to-the-west displacement and rotated a block that encompasses the Resolution deposit by ~25° to the east-northeast.

East of Devils Canyon, extending at least to the Globe mining district, mapping and drilling document major N-S-striking normal faults, which exhibit mainly down-to-the-east displacement. Maher (2008) has shown that these faults are part of a sequence of faults that have resulted in hyperextension and dismemberment of the Miami-Inspiration porphyry copper system.

The present-day geomorphology of the Superior district and immediate surrounding area can be attributed to N- to NW-trending, down-to-the-west, Basin and Range-style normal faults with Tertiary to Quaternary movement. These include the Concentrator, Main, and Conley Springs faults (Fig. 3). The Concentrator fault displaces the Magma vein to an as yet unknown location and defined the western limit of production in the Magma mine.

### Geology of the Resolution Deposit

The following description of the geology and structure within the Resolution deposit builds on the remarkably complete foundation provided by Manske and Paul (2002), considering the limited drill information that was available at the time. Unsurprisingly, additional deeper drilling has revealed even more complexity than they envisioned. This deeper drilling has also shifted emphasis to the Precambrian rocks which are now known to host more than half of the deposit.

#### *Proterozoic rocks*

Pinal Schist is intersected in several deep drill holes below the 1% Cu Shell (Figs. 4, 5). Less than 25 m of siltstone of the Pioneer Formation, the base of the Apache Group, overlies the Pinal Schist, above which it is intruded by a thick (>200 m) diabase sill (the lower sill). Remnants of Pioneer Formation in the lower section of the sill occur as thin, discontinuous lenses of siltstone. The lower sill appears to have preferentially intruded the paraconformable contact between the Pioneer Formation and Dripping Spring Quartzite, as its upper

contact is normally along the basal Barnes Conglomerate member of the Dripping Spring Quartzite, a well-rounded quartz cobble conglomerate which is an infallible marker horizon readily distinguished in drill core. A thick (>100 m) section of the Dripping Spring Quartzite overlies the Barnes Conglomerate member, comprising a lower unit of medium- to coarse-grained quartz and feldspathic arenite and an upper unit of interbedded feldspathic siltstone and fine- to medium-grained quartz and feldspathic arenite. A relatively continuous diabase sill (the middle sill) has intruded the upper unit of the Dripping Spring Quartzite, its upper contact commonly near the paraconformable contact between the upper Dripping Spring Quartzite and the Mescal Limestone, the latter having been intruded by additional discontinuous sills. Basalt flows overlying the Mescal Limestone have only been preserved near the South Boundary fault, and the Troy Quartzite is not present within the graben.

#### *Paleozoic sedimentary rocks*

Within the graben, the Paleozoic section has been significantly attenuated, and in some areas, completely removed by erosion (Figs. 4, 5). Less than 50 m of Bolsa Quartzite, a medium- to coarse-grained quartz arenite, disconformably overlies diabase in the north and western sectors of the down-dropped block, succeeded upwardly by the Martin Formation and eroded remnants of the Escabrosa Limestone. The Martin Formation and Escabrosa Limestone are altered to skarn in all areas of the down-dropped block tested by drilling. Quartz sandstone beds 30 to 40 m above the base of Martin Formation can be recognized in drill core, providing the only marker horizon discernible in the skarn. The maximum thickness of skarn is approximately 200 m, less than the cumulative thickness of the Martin Formation and Escabrosa Limestone in nearby outcrop, suggesting that the Pennsylvanian Naco Group has been completely eroded within the graben.

#### *Cretaceous volcanic and sedimentary rocks*

Cretaceous sedimentary, volcanoclastic, and volcanic rocks host the uppermost 17% (by wt) of material within the 1% Cu Shell and host almost the entire advanced argillic zone. The Cretaceous section is divided into two units, Kqs and Kvs. Two subunits are recognized in the Kvs but the transition between these units is poorly understood and not interpreted on cross sections. They therefore share the Kvs label.

*Quartzose sandstone (Kqs):* The basal Cretaceous section comprises interbedded quartzose sandstone and siltstone up to 150 m thick lying on the Paleozoic or Precambrian formations with a slight angular unconformity. This unit is absent from the southern and eastern sectors of the graben (Fig. 4). U-Pb ages for sedimentary zircons from the sandstone define a maximum age of ~97 Ma (Table 1; Zulliger, 2007).

*Andesitic volcanoclastic rocks (Kvs):* The andesitic Kvs unit is restricted to the west and northwest sector of the graben and comprises a sequence of up to 1 km of graywacke, conglomerate, and lesser lava flows and tuff (Schott, 1994; Manske and Paul, 2002; Ballantyne et al., 2003; Zulliger, 2007). The upper part of the section is dominated by andesitic to basaltic volcanoclastic rocks, whereas the lower part has a transition into discontinuous conglomerate beds containing cobbles of quartzite with less common limestone cobbles; clasts of Pinal

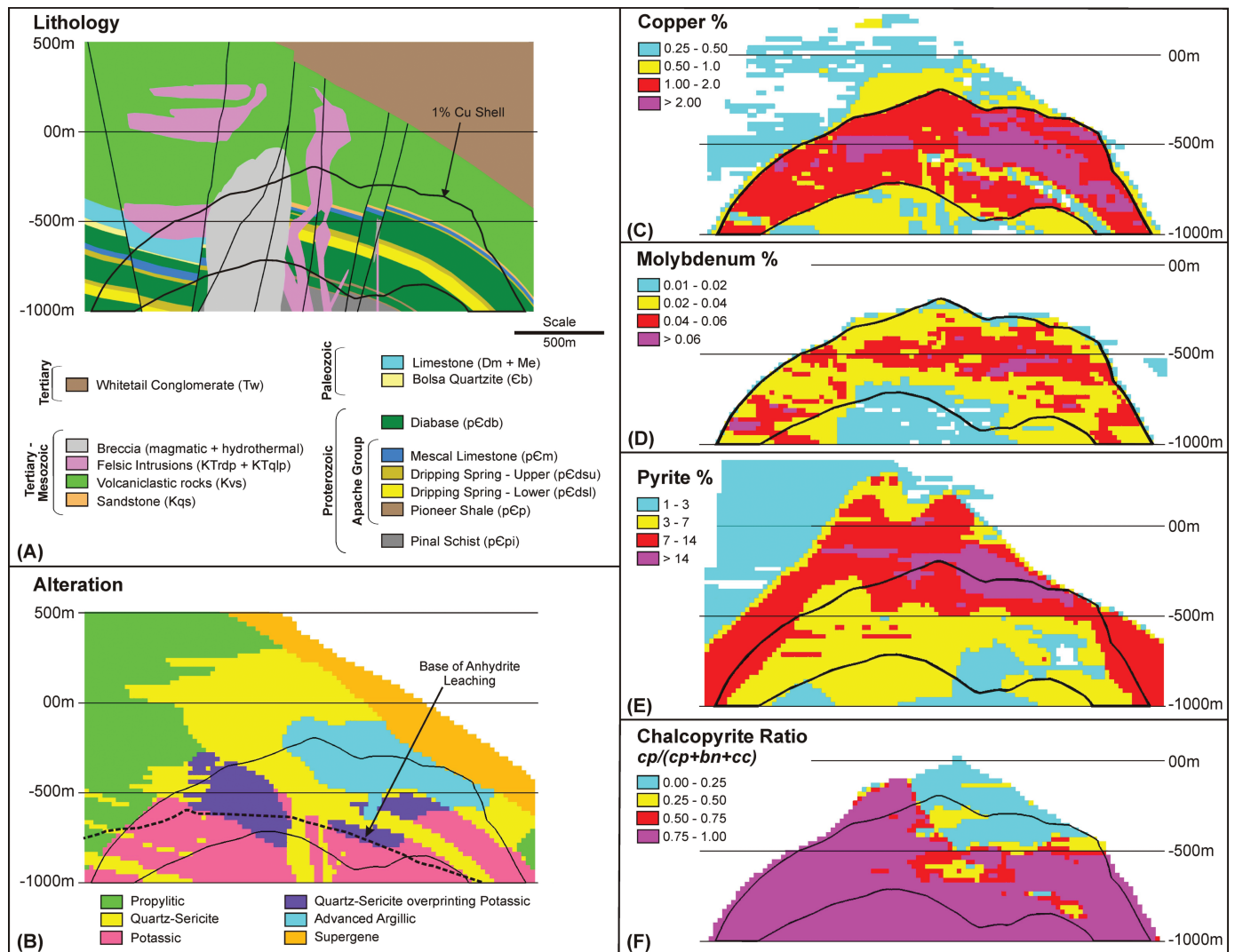


FIG. 5. Section through the Resolution deposit looking northwest. A. Geology. B. Alteration from the block model. C. Copper grade from the block model. D. Molybdenum grade from the block model. E. Pyrite wt % from the block model. F. Chalcopyrite ratio:  $[cp/(cp + bn + cc)]$  from the block model, clipped to 0.5 % Cu grade-limiting shell.

Schist are rare or absent within the volcaniclastic section. Andesite lava flows are present near the base of the Kvs in the southwest sector. U-Pb dates for zircon from two separate interbedded tuffaceous units within ~250 m of the pre-Whitetail Conglomerate paleosurface demonstrate that most of this sequence is older than ~74 Ma. A 75 Ma primary biotite  $^{40}\text{Ar}/^{39}\text{Ar}$  age and a 74 Ma U-Pb zircon age (Table 1) from intrusions in the Silver King area (Figs. 2, 4) suggest that a volcanic center in the Silver King area may have been a source area for the andesitic Kvs.

**Felsic volcanic rocks (Kvs):** A voluminous sequence of dacitic to rhyodacitic tuffaceous rocks dominates the eastern and southern parts of the graben. Notably, these rocks lie on thinned Kqs or unconformably on Proterozoic formations. The volcanic rocks are characterized by clasts of schist, quartzite and, less commonly, diabase and quartz-phyric porphyry, in a tuffaceous matrix composed of broken quartz and feldspar crystals. Upper sections of the sequence are typically matrix dominated while lower sections tend to comprise

coarser clast-supported units of identical composition with local fine-grained tuffaceous interbeds. The felsic volcanic rocks are interpreted by R.H. Sillitoe (pers. commun., 2006) to represent phreatomagmatic eruption products from one or more nearby diatreme vents. Four U-Pb dates from a variety of lithofacies range from 67 to 66 Ma, demonstrating a younger age than the andesitic volcaniclastic rocks to the north and west (Table 1; Zulliger, 2007).

#### Laramide intrusive rocks

Laramide intrusive rocks host 15% of the material within the 1% Cu Shell. These intrusions are considered to be predominantly pre- to early mineral, as they are not observed to cut early quartz-molybdenite or younger veinlets. The intrusions are mostly present within a 1,000-m-wide, E-NE-trending corridor through the center of the deposit. Three intrusive rock types have been identified based on phenocryst assemblages. U-Pb dates from six intrusive rock samples have yielded dates ranging from 69 to 64 Ma, confirming the close

TABLE 1. Radiometric Ages for Superior District Samples

Sample ID	Description	Age (Ma)	Error (2 $\sigma$ )	Laboratory <sup>3</sup>
U-Pb ages for zircons in stratified rocks				
RESSA, 1824.68-1824.86 m	Detrital zircons in Kqs	96.8	2.2	ALC
RES23, 972.3-973.2 m	Zircon in andesitic Kvs	74.1	2.4	ALC
RES24, 824.6-826.2 m	Zircon in andesitic Kvs	74.1	1.2	ALC
RES3, 1205.04-1218.16 m	Zircon in lapilli-crystal tuff in felsic Kvs	67.8	2.3	ALC
RES1, 988.20-1000.91 m	Zircon in lapilli tuff in felsic Kvs	67.6	1.3	ALC
RES2B, 1571.30-1584.45 m	Zircon in lapilli-crystal-lithic tuff in felsic Kvs	67.1	2.3	ALC
RES5D, 1443.49-1456.56 m	Zircon in lapilli-crystal-lithic tuff in felsic Kvs	66.4	1.1	ALC
<sup>40</sup> Ar/ <sup>39</sup> Ar ages for biotite in Silver King Diorite				
SK3, 491447E, 3687589N	Primary biotite in quartz diorite at Silver King mine	74.83	0.33	NMGRL
U-Pb ages for zircons in intrusions				
SK1, 492021E, 3687682N	Zircon in sericitized KTqlp dike at Silver King mine	73.6	1.6	ALC
RES5B, 2086.00-213.15 m	Zircon in eastern KTrdp stock	69.3	1.1	ALC
3653A, RES#3 <sup>1</sup>	Zircon in premineral dike in Magma vein	69.1	4.0	ALC
RES20, 1177.0-1177.5 m	Zircon in KTqlp dike with rare quartz eyes	67.9	1.3	ALC
RES3, 1133.26-1145.56 m	Zircon in KTrdp with K-feldspar megacrysts	67.0	1.7	ALC
RES17F, 1687.0-1688.0 m	Zircon in KTqlp dike with sparse quartz eyes	66.4	0.6	ALC
RES#5, 492016E, 3683628N <sup>1</sup>	Zircon in a KTqlp dike cutting Naco Lst in Queen Creek	66.2	0.8	ALC
S27E, 210.3 m <sup>1</sup>	Zircon in KTrdp dike cutting Kvs	65.0	0.7	ALC
RES2A, 2237.6-2238.7 m <sup>1</sup>	Zircon in coarse-grained KTrdp below 1% Cu shell	64.1	1.9	ALC
A4, 2017.37 m <sup>1</sup>	Zircon in KTrdp dike within Superior East deposit	63.8	1.2	ALC
Re-Os ages for molybdenite in veins				
RES1B, 1825.60-1825.67 m	Quartz-moly vein cutting breccia	65.1	0.3	AIRIE
RES3B, 1551.5-1551.7 m	Banded quartz-moly vein cutting felsic Kvs	64.9	0.2	AIRIE
RES5B, 2082.10-2082.20 m	Quartz-moly vein in eastern KTrdp stock	63.9	0.2	AIRIE
<sup>40</sup> Ar/ <sup>39</sup> Ar ages for biotite in altered rocks				
RES7A, 2251.0-2251.1 m	Biotite replacing mafic minerals in diabase	63.53	0.38	PCIGR
RES1B, 1733.6-1733.7 m	Biotite in matrix of hydrothermal breccia	63.19	0.39	PCIGR
RES2A, 2237.6-2238.7 m	Biotite phenocrysts in coarse-grained KTrdp below 1% Cu shell	63.10	0.11	NMGRL
Highway 177, 490923E, 3682389N	Biotite clots along a vein in Mescal Limestone	62.30	0.15	NMGRL
RES5, 1806.2-1806.3 m	Biotite in matrix of hydrothermal breccia	62.05	0.34	PCIGR
<sup>40</sup> Ar/ <sup>39</sup> Ar ages for sericite in altered rocks				
RES5D, 1704.0-1704.1 m	Muscovite after biotite in KTrdp with quartz-sericite alteration	63.25	0.46	PCIGR
RES2A, 2215.4 m	Sericite in KTrdp with potassic alteration, phyllic overprint	62.85	0.30	NMGRL
RES7B, 2051.1-2051.2 m	Sericite in breccia with quartz-sericite alteration	61.95	0.34	PCIGR
RES5B, 2103.0-2103.1 m	Sericite in KTrdp with quartz-sericite alteration, adv. argillic overprint	61.93	0.34	PCIGR
<sup>40</sup> Ar/ <sup>39</sup> Ar ages for alunite in veins and a breccia				
RES3, 1275.34 m	Alunite in Kvs	62.3	0.4	PCIGR
RES3, 1275.34 mR	Alunite in Kvs	61.67	0.36	PCIGR
RES9J, 1378.3-1378.5 m	Quartz-alunite-chalcocite-digenite veinlets in feldspathic Kvs	61.3	1.8	NMGRL
RES15A, 1601.8-1602.0 m	Fine-grained alunite-dickite-kaolinite as breccia infill in KTrdp dike	60.4	1.2	NMGRL
RES5H, 1742.9-1743.0 m	Hypogene alunite vein in eastern KTrdp stock	51.67	0.29	PCIGR
RES5H, 1742.9-1743.0 mR <sup>2</sup>	Hypogene alunite vein in eastern KTrdp stock	51.22	0.49	PCIGR
RES13, 1968.18 m	Hypogene alunite vein in eastern KTrdp stock	49.46	0.57	PCIGR
RES13, 1968.18 mR <sup>2</sup>	Hypogene alunite vein in eastern KTrdp stock	49.39	0.38	PCIGR
Re-Os ages for pyrite in late veins in Kvs				
RES9J, 1389.0-1389.1 m	Massive pyrite vein with dickite infill in Kvs	51.4	0.2	AIRIE
RES9J, 1394.1-1394.2 m	Massive pyrite vein with dickite infill in Kvs	22.97	0.10	AIRIE
RES9J, 1394.1-1394.2 mR <sup>2</sup>	Massive pyrite vein with dickite infill in Kvs	22.77	0.08	AIRIE
<sup>40</sup> Ar/ <sup>39</sup> Ar ages for sanidine within Whitetail Conglomerate				
RES21, 1789.8-1790.1 m	Sanidine in Tw in airfall tuff 80 m above base	24.29	0.12	NMGRL
RES20, 757.0-758.0 m	Sanidine in Tw in airfall tuff 170 m above base	21.97	0.06	NMGRL
<sup>40</sup> Ar/ <sup>39</sup> Ar ages for igneous biotite within Whitetail Conglomerate				
RES11, 651.55-651.66 m	Biotite in Tw in fine volcanic sediment 350 m above base	21.77	0.32	AIRIE

<sup>1</sup> Age from Seedorff et al. (2005b)<sup>2</sup> "R" following a sample ID indicates a repeated age determination on the same concentrate<sup>3</sup> Abbreviations: ALC = Arizona LaserChron Center at University of Arizona, AIRIE = AIRIE Program at Colorado State University, PCIGR = Pacific Center for Isotopic and Geochemical Research at University of British Columbia, NMGRL = New Mexico Geochronology Research Laboratory at New Mexico Institute of Mining and Technology; Kqs = quartzose sandstone, KTrdp = rhyodacite porphyry, KTqlp = quartz latite porphyry, Kvs = andesitic/felsic volcanoclastic rocks, Tw = Whitetail Conglomerate

temporal relationship with the felsic Kvs volcanic rocks (Table 1; Seedorff et al., 2005b; Stavast, 2006; Zulliger, 2007).

*Rhyodacite porphyry (KTrdp)*: Rhyodacite porphyry, the most voluminous of the Laramide intrusive rock types, forms a stock-like body (~400 × 400 m) in the eastern part of the deposit and a smaller stock (~200 × 200 m) to the west, as well as dikes and lesser sills throughout the deposit. Typically, phenocrysts of quartz, plagioclase, K-feldspar, and lesser biotite make up 50% of this rock and are set in an aphanitic groundmass. A distinctive variant of the rhyodacite porphyry is characterized by K-feldspar phenocrysts up to 30 mm in length. Cross-cutting relationships between the K-feldspar megacryst-bearing variant and other variants have not been observed as yet.

*Quartz latite porphyry (KTqlp)*: Quartz latite porphyry is less voluminous than rhyodacite porphyry and occurs only as dikes. This rock type has fewer quartz phenocrysts than the rhyodacite. Where less intensely altered, quartz, plagioclase, and lesser biotite and hornblende are present as phenocrysts, but the matrix has commonly been variably altered to biotite, coarse to fine quartz, and white phyllosilicate minerals. Quartz latite dikes are locally observed to truncate early quartz-only veins present in rhyodacite porphyry.

*Latite porphyry (KTlp)*: Latite porphyry is present only as minor dikes. This porphyry has a high proportion of feldspar phenocrysts to matrix, and hence a crowded texture when compared to the other dikes and exhibits a notable absence of quartz phenocrysts. The latite porphyry has not been observed in contact with other Laramide intrusions.

### Breccias

Two variable heterolithic fragmental units have been identified at Resolution and together host ~10 vol % of the mineralization within the 1% Cu Shell. These breccias lie within the same E-NE-trending corridor that contains the Laramide intrusions. Quartz-phyric porphyry occurs both as clasts in the breccias and as dikes which crosscut the breccias, temporally bracketing breccia formation (R.H. Sillitoe, pers. commun., 2006).

*Hydrothermal breccia*: Two main bodies of hydrothermal breccia occur within the deposit, a 500- × 100-m east-west body wrapping around the northern margin of the eastern rhyodacite porphyry stock and a discrete 400- × 200-m pipe-like body in the southwest sector. Both bodies may be either clast or matrix supported and contain subangular to subrounded clasts of all of the Precambrian to Paleozoic lithologies seen in the deposit. The most common clast type is typically the rock unit adjacent to the breccia, so the breccias maintain the local stratigraphy in a gross sense. Nonetheless, a few large clasts have been noted tens of meters above or below their original stratigraphic position. At lower elevations the breccia matrix contains abundant fine-grained secondary biotite with lesser quartz + anhydrite ± rutile. Locally quartz-only vein fragments and clast-restricted, early quartz-only veins suggest an early mineral timing (J.M. Proffett, pers. commun., 2001; Zulliger, 2007).

*Intrusion breccia*: This breccia is characterized by an igneous matrix that is texturally and compositionally similar to rhyodacite porphyry; the breccia bodies locally appear to grade into coherent rhyodacite porphyry. Apache Group sedimentary rocks, Proterozoic diabase and schist are all common clast types. The intrusion breccia is typically clast supported,

forming small, sporadic, irregularly shaped bodies. Zulliger (2007) suggested that the breccias may be feeders for the felsic tuffs within the Kvs sequence. Because these igneous breccias are normally dominated by siliceous rock types, they tend to have lower copper grades than the hydrothermal breccia. Intrusion breccia locally contains clasts of hydrothermal breccia, indicating a younger age for the intrusion breccia.

Another type of hydrothermal breccia has been distinguished but it is volumetrically minor. In these breccias, clasts containing truncated quartz-molybdenite veins are in turn cut by quartz-molybdenite veins, thus assigning an intraquartz-molybdenite-stage timing to their formation. Small bodies of hydrothermal crackle breccia, with fragments that have not been rotated, also occur within various rock types throughout the deposit.

### Postmineral sedimentary and volcanic rocks

*Whitetail Conglomerate (Tw)*: Whitetail Conglomerate forms a NE-thickening sequence of predominantly poorly sorted conglomerates up to 1.3 km thick overlying the deposit. A basal ferricrete member (Manske and Paul, 2002) comprises detritus primarily from the immediately underlying leached capping and may attain a thickness of up to 60 m. New high-precision biotite and sanidine  $^{40}\text{Ar}/^{39}\text{Ar}$  age determinations for samples from interbedded tuffs in the lower to middle sections of the conglomerate range from  $24.29 \pm 0.12$  to  $21.77 \pm 0.32$  Ma (Table 1).

*Apache Leap tuff (Tal)*: The Miocene Apache Leap tuff is a biotite-phyric dacite ash-flow tuff that is 350 to 500 m thick above the deposit and dips ~12° to the northeast. Pumice fragments are progressively flattened with depth (Peterson, 1961). The Apache Leap tuff has been dated by the  $^{40}\text{Ar}/^{39}\text{Ar}$  method to be 18.6 Ma (Ferguson et al., 1998).

### Structure

The E-NE-trending North Boundary fault is one in a series of at least three parallel faults bounding the graben on the north. In the northwest portion of the graben, the North Boundary fault and related faults displace the base of Paleozoic strata by ~500 m (Fig. 4), but because of differential erosion of the Paleozoic section within the graben, faulting accommodates ~1 km of Cretaceous strata.

Intercepts of the West Boundary fault from three recently completed geotechnical drill holes provide data along 1.5 km of strike and define a southeasterly strike and a dip of ~85° to the southwest. Displacement along the West Boundary fault is not well constrained, but ~1 km of Cretaceous strata are preserved east of the fault. Drilling within the graben documents a dramatic thinning of these Cretaceous strata from west to east, with less than 300 m of Kvs strata and no Kqs present in the eastern part. Because the North and West Boundary faults do not continue with such significant offsets outside the graben, they appear to be linked kinematically.

Resolution Copper Mining has not completed any drill holes across the deeper portions of the South Boundary fault. As described by Paul and Manske (1998), the South Boundary fault is a 120- to 150-m-wide complex fault zone with major fault strands on the hanging-wall and footwall sides, dipping northward at 60° to 90°. Fault offsets are less well constrained but are similar to those along the North Boundary fault.

Determining the detailed structural geology within the deposit is challenging because the deposit is known only from drilling. Most faults within the deposit are inferred based on stratigraphic offsets in adjacent drill holes but critical additional support comes from oriented drill core. More than 50,000 orientations for bedding, stratigraphic and igneous contacts, faults, discrete shears, slickenside lineations, joints, and foliation have been recorded in drill core, many of them with the aid of an acoustic bore hole imaging tool. Orientations for key structure types within the immediate deposit area are summarized in the stereonet of Figure 6.

Most faults within the graben strike north to north-northeast, dip steeply west, and show down-to-the-west displacement. These conclusions are confirmed by pole plot clusters for 1,650 slickensided shears, and lineations along those shears, recorded in oriented core (Fig. 6B, C). Uplift on the east side of the N-trending faults has resulted in significant to complete removal of the Paleozoic section in the east-central portion of the deposit (Fig. 5A). Changes in the thickness of

diabase sills across some of the N-trending faults suggest they originated as much older inflation faults that served as plumbing for the diabase sill complex. None of the northerly trending faults described here has been shown to have significant offsets outside the graben.

A prominent fault that trends east-west through the middle of the deposit has been intruded by rhyodacite porphyry forming a dike. This fault is interpreted as a strike-slip fault accommodating dilation and intrusion. Although postmineral faults clearly cut the deposit, the continuity of grade and alteration style across these structures (Fig. 5B-F) suggests that any postmineral offset is modest.

### Hydrothermal Alteration

#### Potassic alteration

Potassic alteration of variable intensity affects at least 5 km<sup>3</sup> of rock (2 × 2.5 km in plan × 1 km depth) within and surrounding the Resolution mineralization, extending to the

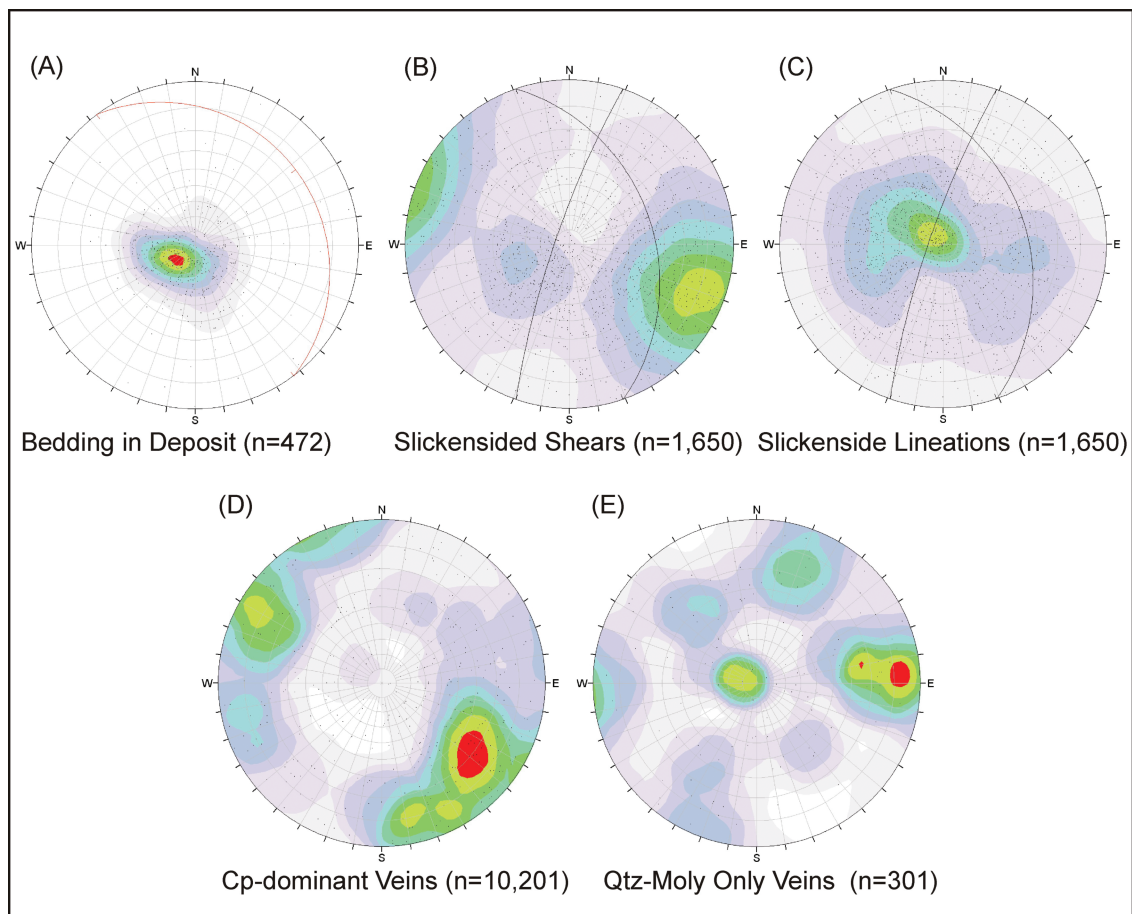


FIG. 6. Lower hemisphere equal-area projections, showing pole plots and great circles of features measured in oriented core. Contours from Fisher probability fields calculated using the Kent distribution method and a 5% area counting circle using the "Dips" software. A. Stereonet showing bedding attitudes within the 1% Cu shell. Data show modest average north-east dip. B. Stereonet of slickensided shears showing dominance of steep W dipping faults with a smaller cluster of E-NE-dipping features that represent parallel shears. C. Pole plot of lineation orientation with great circles representing slickensided shears from (B). Data show that lineations are primarily along the main trend of N-NE-striking high-angle faults, and that the recorded movement along these faults is primarily dip-slip. D. Pole plot of veins containing chalcopyrite as the dominant copper-bearing mineral, showing variable orientation but steep average dip and a northeast strike. E. Pole plot of quartz-molybdenite veins, showing variable orientation with steep average dip and northerly strike.

northern and southern boundary faults of the graben (Figs. 3, 4). Secondary biotite is intensely developed in diabase, comprising up to 46% of the rock, and to a much lesser extent in porphyry intrusions, quartzose sedimentary rocks, and Kvs. K-feldspar alteration is more prevalent in porphyry intrusions and Kvs than in diabase. Anhydrite is a major component of the potassic alteration assemblage in the core of the system but has been dissolved by ground water above a surface dipping 20° to the east-northeast that cuts across the 1% Cu Shell (Fig. 5B). Hydrothermal magnetite is common on the southern and northwestern flanks of the deposit but scarce elsewhere.

Potassic alteration is pervasive in the deeper zones of the deposit where hydrothermal biotite and K-feldspar survived subsequent hydrolytic alteration events. In addition, cryptic K-feldspar alteration, recognizable with sodium cobaltinitrite staining, is widespread in rocks affected by epidote and chlorite alteration in the propylitic zone (see below). Potassically altered diabase contains lower concentrations of Ca, Fe, Na, Ti, and Mn, and higher concentrations of K, S, As, Ag, Au, Cu, and Mo, relative to unaltered diabase (Table 2).

A general sequence of veining has been deciphered for the numerous vein types associated with potassic alteration. Early green biotite-anhydrite veinlets with brown biotite halos (present in diabase) are cut by quartz-anhydrite veins with variable amounts of biotite, chalcopyrite, pyrite (or) bornite, magnetite, and, locally, traces of molybdenite and carbonate. In diabase from the southern sector of the deposit, veins from this stage are strongly rich in magnetite. Next, chalcopyrite-rich quartz-anhydrite veins with variable amounts of K-feldspar, biotite, sericite, and molybdenite were emplaced, followed by the main molybdenite-bearing stage of quartz-anhydrite veins which also contain variable amounts of chalcopyrite, K-feldspar, biotite, and sericite; both vein types locally contain pyrite or bornite.

An episode of synmineralization ductile deformation occurred during the late stages of potassic alteration (Ballantyne et al., 2003). This deformation is expressed as a generally shallowly dipping (after correcting for 25° ENE postmineral tilt),

planar foliation of grains, and patches of secondary biotite, and as sympathetic folding and boudinage of the veins described above (Schwarz, 2010). In hydrothermal breccia, foliation is also manifested as rotation and alignment of elongate clasts; secondary biotite grains in diabase clasts are all aligned with the foliation. This ductile deformation, only observed to affect diabase and hydrothermal breccia, is most intense in the central part of the deposit and is interpreted as the product of local strain imposed by the intrusion of a roughly cylindrical stock inferred at depth, with attendant volume expansion of rock undergoing hydrothermal alteration below the brittle-ductile transition (Fournier, 1999). The phenomenon is particularly well developed at Resolution due to the ductile nature of the intensely biotite-altered diabase, which promoted plastic deformation under stress conditions that would have caused brittle deformation in the siliciclastic and volcanoclastic rocks encasing it.

#### *Propylitic alteration*

The Resolution deposit is surrounded by a halo of propylitic alteration defined by mineral assemblages including chlorite and epidote (Fig. 5B). In a few distal holes, epidote is absent but calcite is present, suggesting that a chlorite-calcite subzone may lie between rocks containing epidote and unaltered rock. On the southern margin of the deposit, potassic alteration in diabase was preceded by an alteration episode where pyroxene and hornblende were replaced by amphibole and magnetite, and, locally, veins of actinolite, quartz, and magnetite are present. However, a continuous, actinolite-bearing subzone has not been recognized between the potassic and propylitic zones. At its inner edge, the chlorite-epidote zone gives way to pervasive quartz-sericite-pyrite alteration at higher elevations and to rocks with strong secondary biotite alteration at depth.

Albite has not been noted petrographically in the chlorite- and epidote-bearing rocks at Resolution, but K-feldspar is abundant. The K-feldspar, which locally constitutes more than 25% of the rock volume, commonly occurs as small equant, untwinned grains in the groundmass but also occurs with epidote in former plagioclase sites and in quartz-carbonate-epidote veins. As shown by the data in Table 2, propylitized diabase contains lower concentrations of Ca, Fe, and Na and higher concentrations of K, S, Ag, As, Au, Cu, Mn, Pb, and Zn than unaltered diabase. These variations are similar to those reported for other porphyry copper deposits (e.g., Panguna; Ford, 1978), except for the atypically high potassium in the propylitic zone at Resolution.

The outer boundary of the pyrite halo lies within the chlorite-epidote zone, and pyrite abundance increases strongly inward across the zone. Manganese oxides are particularly common within the chlorite-epidote zone immediately outside the pyrite halo. Hematite is common within the chlorite-epidote zone, both within and outside the pyrite halo. Quartz veins are scarce within the propylitic zone, but narrow quartz-epidote-carbonate veins are present and locally contain various combinations of pyrite, chalcopyrite, galena, and sphalerite.

#### *Quartz-sericite-pyrite alteration*

Quartz-sericite-pyrite alteration overprints potassic alteration at depth and propylitic alteration laterally and is overprinted

TABLE 2. Compositional Variation in Diabase

Sample ID	Unaltered	Potassic	Propylitic	Quartz-sericite	Adv. argillic
From (m)	16, 20	RES-002A	RES-016	RES-017G	RES-017A
Length (m)	N/A	1825.55	1195.90	1669.90	1750.30
		146.45	32.20	41.43	37.90
Al (%)	7.03	5.98	6.04	5.70	7.66
Ca (%)	5.36	2.51	2.93	0.10	0.23
Fe (%)	9.90	6.78	6.54	5.80	4.92
K (%)	1.91	3.61	4.62	3.30	3.17
Mg (%)	2.65	2.63	3.06	0.60	0.53
Na (%)	2.20	0.16	0.10	0.05	0.06
S (%)	<0.01	5.28	2.81	6.40	6.12
Ti (%)	0.99	0.37	0.60	0.50	0.71
Ag (ppm)	<0.05	1.06	5.75	1.80	4.36
As (ppm)	2.2	2.6	10.2	69.3	31.3
Au (ppb)	2	31	188	36	146
Cu (ppm)	109	12939	650	16802	31298
Mn (ppm)	1588	411	3173	77	40
Mo (ppm)	1	142	1	278	859
Pb (ppm)	12	4	276	<3	35
Zn (ppm)	95	83	1398	20	136

by advanced argillic assemblages in the upper levels of the Resolution system. In areas tested by drilling, quartz-sericite-pyrite alteration overprints a large volume of the potassic alteration and some of the propylitic alteration. The remaining volume of pervasive quartz-sericite-pyrite alteration exceeds 1 km<sup>3</sup>; however, a large additional volume has probably been removed by erosion because quartz-sericite-pyrite alteration (Fig. 5B) is extensive at the pre-Whitetail Conglomerate erosion surface (Fig. 5A).

Quartz-sericite-pyrite alteration affects all premineral units within the deposit to varying degrees but is best developed in the Cretaceous and uppermost Proterozoic units. The siliceous rock types (Dripping Springs Quartzite, Bolsa Quartzite, Kqs, KTqlp, and KTrdp) are preferentially altered to quartz-sericite-pyrite at deeper levels.

Sericite in the Resolution deposit is mostly a moderately phengitic muscovite. Shortwave infrared spectroscopic analysis by CSIRO's HyChips™ system indicates that the most common location for the Al-OH peak for white mica in Resolution samples lies at about 2,207 nm, i.e., closer to end-member muscovite (2,200 nm) than to phengite (2,220 nm). Spatial zoning of sericite compositions has not been demonstrated to date.

The quartz-sericite-pyrite alteration in the Resolution deposit occurs as quartz-pyrite ± Cu sulfide veins with texturally destructive sericite halos, i.e., D-type veinlets (Gustafson and Hunt, 1975), and can be sufficiently intense so as to completely obliterate protolith textures. Massive and/or pervasive silicification is uncommon. Quartz-sericite-pyrite alteration is accompanied by minor fluorite, anhydrite, and rutile (Manske and Paul, 2002; Harrison, 2007; Zulliger, 2007; Schwarz, 2010; Winant, 2010).

Sericite appears to have been partially replaced by kaolinite in large rock volumes without associated diagnostic advanced argillic minerals. The sericite-kaolinite assemblage may represent a transition from quartz-sericite-pyrite to advanced argillic alteration, as described by Seedorff et al. (2005a). As indicated in Table 2, quartz-sericite-pyrite-altered diabase contains lower concentrations of Ca, Fe, Mg, Na, Mn, Pb, and Zn and higher concentrations of S, As, Ag, Au, Cu, and Mo than unaltered diabase.

#### *Advanced argillic alteration*

Advanced argillic assemblages are almost entirely contained within quartz-sericite-pyrite-altered rock volumes (Fig. 5B), mainly in the upper Kvs-hosted parts of the deposit (Fig. 5A). About half the volume of rock affected by advanced argillic alteration lies above the top of the 1% Cu Shell (Fig. 5B). Dickite and lesser amounts of topaz extend up to 1.5 km laterally from the center of the hydrothermal system along favorable strata, notably within Kqs and Cambrian Bolsa Quartzite in the northwest sector. Topaz alteration also forms a halo up to 300 m wide immediately above the 1% Cu shell as well as in strongly fractured zones within the 1% Cu shell. Kaolinite, as determined by near-infrared spectroscopy, and pyrite are the most abundant alteration minerals within the advanced argillic assemblage at Resolution, but dickite is the mineral diagnostic of advanced argillic alteration most easily recognized in drill cores. In decreasing order of abundance and distribution, alunite, zunyite, woodhouseite, and

pyrophyllite are also present (Troutman, 2001; Manske and Paul, 2002; Harrison, 2007; Zulliger, 2007; Winant, 2010). These minerals are typically associated with 10 to 20 wt % pyrite and 25 to 100 ppm arsenic; enargite is rarely present. Diabase affected by advanced argillic alteration has a similar composition to diabase affected by quartz-sericite-pyrite alteration (Table 2).

#### *Skarns*

Destruction of original carbonate minerals in Proterozoic and Paleozoic carbonate units is complete within the 1% Cu Shell. Volume reduction during skarn formation may contribute to the reduced thickness of the Paleozoic stratigraphic section seen at some locations within the downdropped block at Resolution; such volume reduction due to skarn formation was documented within similar host carbonates at Christmas (Perry, 1969).

*Magnesian skarn:* Magnesian skarn occurs primarily within dolomitic portions of the Mescal Limestone and in the lower portion of the Martin Limestone; anhydrous magnesian skarn has not been identified within the Resolution deposit. The most characteristic minerals of the magnesian skarn are tremolite and talc but anhydrite, chlorite, serpentine, magnetite, and hematite are also typically present. Magnetite is usually partially altered to hematite.

*Calcic skarn:* In limestone beds, early assemblages of andraditic garnet ± diopside ± wollastonite are partially to completely overprinted by hydrous minerals including chlorite, actinolite, epidote, and calcite. Biotite hornfels formed locally in interbedded silty or shaley limestones. Magnetite is rare to absent in retrograde calcic skarn.

*Quartz-pyrite-altered skarn:* Intense alteration to an assemblage of quartz-sericite-pyrite ± kaolinite ± dickite has affected some retrograde skarns. In some drill core intervals relict bands of pyrite and chalcopyrite are the only evidence of a former skarn. Calcium and magnesium have been strongly leached and are typically present in amounts of <1 wt %.

## Mineralization

### *Copper mineralization*

Copper grade and mineralogy at Resolution are strongly dependent on both lithology and the predominant alteration type (Fig. 5A-C). Copper grades are higher than average in carbonate host rocks, diabase, breccia, and volcanoclastic rocks and lower in quartzite, quartzose sandstone, and Laramide intrusive rocks (Table 3).

Chalcopyrite is the dominant copper mineral in the deposit, comprising ~65 wt % of the copper in the 1% Cu Shell. Chalcopyrite is commonly the only copper sulfide mineral in rocks that exhibit exclusively potassic alteration. However, potassically altered rocks without a quartz-sericite-pyrite overprint are rare and rocks with a quartz-sericite-pyrite overprint typically have significantly higher copper grades and a chalcopyrite-bornite-pyrite sulfide assemblage. A late, high sulfidation assemblage consisting of bornite, chalcocite, digenite, and pyrite is spatially associated with sericite ± kaolinite alteration, with or without other diagnostic advanced argillic minerals.

TABLE 3. Average Grades for the 1% Cu Shell by Lithology, Alteration, and Mineralization Type

Lithology-alteration-mineralization type	(%) Cu	(%) Mo	(g/t) Ag	Lithology (vol %)
Kvs	1.58	0.034	3.68	12%
Kqs	0.95	0.038	4.49	5%
Diabase	1.58	0.038	3.02	36%
Breccia	1.64	0.033	2.61	10%
Laramide intrusion, chalcopyrite dominant	0.97	0.039	2.52	9%
Laramide intrusion, chalcocite dominant	1.42	0.025	2.18	6%
Paleozoic and Proterozoic quartzite	0.78	0.044	3.24	12%
Retrograde skarn	1.73	0.035	3.87	8%
Quartz-pyrite-altered skarn	3.16	0.054	8.17	2%

Kqs = quartzose sandstone, Kvs = andesitic/felsic volcanoclastic rocks

Copper-bearing skarns make up 10% of the material within the 1% Cu Shell (Table 3). Magnesian skarns carry chalcopyrite and lesser bornite, whereas bornite is rare in calcic skarns. Magnetite and/or hematite tend to be approximately as abundant as the copper sulfides in magnesian skarns but are rare to absent in calcic skarns. Both magnesian and calcic skarns typically carry ~0.1% zinc as sphalerite. Quartz-pyrite-altered skarns carry high-grade copper mineralization including chalcopyrite, bornite, chalcocite, and digenite, and >15 wt % pyrite.

Figure 7 shows an example of how copper mineralogy and grade change with depth and lithology in an individual drill hole. Drill hole RES-17F is collared above the center of the deposit and inclined toward the northeast. As shown, chalcopyrite and bornite are the predominant copper sulfide minerals at most depths but significant chalcocite and traces of enargite are present at shallower depths (Fig. 7, based on QEMSCAN analysis).

#### Molybdenum mineralization

Molybdenum averages ~370 ppm within the 1% Cu Shell and occurs most commonly in quartz veins with molybdenite concentrated at vein edges, i.e., B-type veinlets (Gustafson and Hunt 1975). These veins contain variable amounts of chalcopyrite and are considered to be temporally transitional between potassic and quartz-sericite-pyrite alteration (Schwarz, 2010). Overall there is a good spatial correlation between the 1% Cu Shell and the >100 ppm Mo grade shell (Fig. 5C, D) but this correlation is absent at a local scale. Quartz-rich sedimentary rocks and Laramide intrusive rocks (i.e., silica-rich lithologies) commonly contain molybdenum grades greater than the deposit average.

#### Veining and paragenesis

The veining sequence at Resolution conforms to the general progression of vein emplacement observed in many calc-alkalic porphyry deposits (Gustafson and Hunt, 1975). These veins record the fluid evolution (Fig. 8), characterized by cooling and pH decrease with time. Early veins contain quartz, anhydrite, chalcopyrite, bornite or pyrite, molybdenite, and locally, magnetite, and display K-feldspar and biotite alteration selvages. It is estimated that this stage of veining contributed ~0.3 to 0.7 wt % Cu to the deposit, or roughly 20

#### Copper Distribution in Drill Hole RES-17F

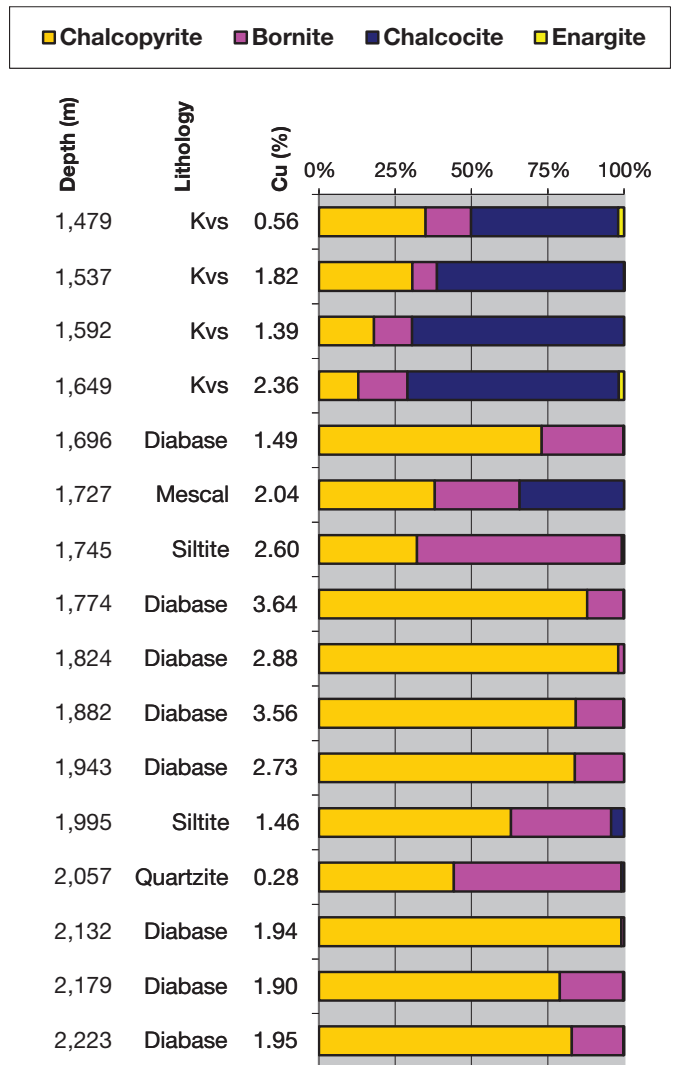


Fig 7. Quantitative evaluation of minerals by scanning electron microscopy (QEMSCAN) analyses of composite samples from drill hole RES-17F. Normalized copper mineralogy, with downhole depths in meters of the start point of sample composites. Drill hole RES-17F is collared above the center of the deposit and drilled to the northeast. Kvs = andesitic/felsic volcanoclastic rocks.

to 45% of the Cu in the 1% Cu Shell (Schwarz, 2010). These veins were affected by an episode of ductile deformation and biotite foliation in the diabase.

The majority of the copper within the resource at Resolution was deposited during the quartz-sericite alteration stage. The early veins with K-silicate selvages described above are cut by a group of veins with sericite selvages whose vein-filling minerals vary with depth. In the lower part of the deposit, the dominant vein-filling minerals are pyrite, chalcopyrite, quartz, anhydrite, and locally, hematite and carbonate (Troutman, 2001; Harrison, 2007; Winant, 2010). Chalcopyrite content in these veins varies, and the chalcopyrite typically precipitated after pyrite. Chalcopyrite is also commonly partially replaced by bornite, chalcocite, and digenite (Fig. 9). In the upper part of the deposit, veins with sericite selvages are dominated by a high



sulfidation assemblage of chalcocite, bornite, digenite, and pyrite, and some have alteration selvages that are transitional to advanced argillic alteration. Most of the chalcocite-digenite mineralization is hosted by Kvs and within the upper levels of Laramide intrusions (Figs. 5E, 8). The lower boundary of the 1% Cu Shell is normally associated with a sharp decrease in the abundance of veins with sericite selvages. In skarns, this stage of veining is represented by pyrite-chalcopyrite veins with alteration halos dominated by chlorite but locally containing epidote, actinolite, talc, sericite, serpentine and calcite.

Hypogene hematite and/or specular hematite occurs in relatively small rock volumes primarily deep in the deposit. Hematite appears to be in equilibrium with chalcopyrite and/or bornite that is associated with well-developed quartz-sericite alteration.

Late-stage veins consist of a high sulfidation assemblage of pyrite, bornite, chalcocite, digenite, quartz, and scarce covellite and enargite and have dickite, kaolinite, and topaz in their selvages. These veins are most abundant in the upper part of the 1% Cu Shell (Fig. 5F) and occupy significant volumes of rock containing >14 wt % pyrite (Fig. 5E). The average pyrite content of the material within the 1% Cu Shell is ~8 wt %.

#### *Gold and silver*

Gold contents within the 1% Cu Shell at Resolution are negligible, averaging ~50 ppb, whereas silver averages ~3.25 ppm. There is an overall spatial correlation between elevated silver concentrations and advanced argillic alteration, suggesting silver substitution within the chalcocite that accompanies advanced argillic alteration. Skarn, especially where subjected to late quartz-pyrite alteration, has above average gold and silver contents (Table 3).

#### *Leached capping and supergene enrichment*

A hematite-dominated leached capping up to 250 m thick overlies the Resolution deposit, dipping east northeast (Fig. 5B). The leached capping is developed in the Cretaceous volcanic rocks, intrusions, and breccias and was formed when the deposit was uplifted and partially eroded sometime prior to ~25 Ma, or the onset of Tertiary basin and range faulting. No significant chalcocite blanket has been identified although locally some modest intersections of secondary chalcocite are present. In the eastern sector of the deposit leached capping shows a transition into hypogene sulfides over a few meters with no intervening secondary chalcocite (Fig. 5B). The mixed oxide-sulfide zone is normally <50 m thick but locally extends farther down faults and fracture zones. Minor amounts of native copper occur in the leached capping.

#### *Age of mineralization*

Twenty-three new radiometric ages for sulfide minerals, and for biotite, sericite, and alunite from rocks that have suffered intense hydrothermal alteration, are reported in Table 1. The Re-Os ages were determined by the AIRIE Program at Colorado State University by methods described by Stein et al. (2000, 2001) and Zimmerman et al. (2008). The biotite, sericite, and alunite ages were determined by the  $^{40}\text{Ar}/^{39}\text{Ar}$  method at the Pacific Center for Isotopic and Geochemical Research at the University of British Columbia and at the

New Mexico Geochronology Research Laboratory at the New Mexico Institute of Mining and Technology.

Re-Os dates were determined for molybdenite from three samples: a quartz-molybdenite vein cutting a hydrothermal breccia, a banded quartz-molybdenite vein cutting a felsic volcanoclastic rock, and a quartz-molybdenite vein cutting the eastern rhyodacite porphyry stock. The Re-Os ages range from  $65.1 \pm 0.3$  to  $63.9 \pm 0.2$  Ma (Table 1; Zulliger, 2007).

New  $^{40}\text{Ar}/^{39}\text{Ar}$  ages are reported for five samples of biotite and for four samples of sericite from hydrothermally altered rocks. The biotite ages range from  $63.53 \pm 0.38$  to  $62.05 \pm 0.34$  Ma and the sericite ages range from  $63.25 \pm 0.46$  to  $61.93 \pm 0.34$  Ma. Biotite phenocrysts from a dike of coarse-grained, potassically altered KTrdp that lies beneath the thickest part of the 1% Cu shell, near the center of the deposit, yield an age of  $63.10 \pm 0.11$  Ma. Zircons from the same dike yield a U-Pb age of  $64.1 \pm 1.9$  Ma.

The Re-Os molybdenite ages and the  $^{40}\text{Ar}/^{39}\text{Ar}$  biotite and sericite ages suggest that the bulk of the copper and molybdenum mineralization at Resolution may have occurred between ~65 and ~64 Ma, and that the system cooled below the argon closure temperatures for biotite and sericite between ~63.5 and ~62 Ma. This magmatic cooling scenario is also supported by the U-Pb and  $^{40}\text{Ar}/^{39}\text{Ar}$  ages, ~64 and ~62.7 Ma, respectively, for the potassically altered KTrdp dike from beneath the center of the deposit.

$^{40}\text{Ar}/^{39}\text{Ar}$  ages for four alunite samples, including one from a quartz-alunite-chalcocite-digenite vein, range from  $62.3 \pm 0.40$  to  $60.4 \pm 1.2$  Ma.  $^{40}\text{Ar}/^{39}\text{Ar}$  ages for two other hypogene alunite samples range from  $51.67 \pm 0.29$  to  $49.39 \pm 0.38$  Ma. A single-sample Re-Os age of  $51.4 \pm 0.2$  Ma for pyrite from a massive pyrite-dickite vein is consistent with the two younger alunite ages and may suggest a later pulse of hydrothermal activity. We are not yet ready to draw conclusions on replicate single-sample Re-Os ages of  $22.97 \pm 0.1$  and  $22.77 \pm 0.08$  Ma for pyrite from another massive pyrite-dickite vein.

## Discussion

#### *Geologic setting*

The Resolution deposit occurs within a long-recognized, E-NE-trending mineral belt that extends for 35 km, from Superior to Globe, and includes numerous copper occurrences (Peterson, 1962; Sell, 1995). Maher (2008) developed a structural reconstruction which indicates that many of the larger copper deposits in the eastern half of the belt are portions of a single porphyry copper system hosted by the Schultze Granite and dismembered by ENE-WSW hyperextension on rotated, flat-dipping faults. However, the Resolution deposit, which lies near the western end of the belt, is hosted mostly by sedimentary rocks and conformable diabase sills; structural interpretations constrained by stratigraphy suggest that extension was modest, and that the deposit has been affected by only about ~25° of postmineral tilting toward the east northeast.

A striking aspect of the local setting of the Resolution deposit is the presence of numerous E-W- to E-NE-trending veins exposed to the west of the deposit (Fig. 2). Drilling has confirmed the predominance of N-NE- to E-NE-trending vein orientations within the deposit (Fig. 6D). Heidrick and

Titley (1982) noted that E-NE-trending veins and dikes are common to many of the mining districts in the Southwest North America porphyry copper province and may reflect E-NE-oriented compression resulting from convergence of the Farallón and North America plates. Variations in vein orientations in the Resolution district may reflect interaction between old structural fabrics and the local stress field at the time of mineralization.

#### *Resolution horst/graben*

A fortuitous aspect of the geology at Resolution is the preservation of Cretaceous sedimentary rocks and tuffs within a local graben. Hammer (1967) suggested a correlation between the Cretaceous rocks at Resolution and those present in the Reed basin east of the Christmas deposit. U-Pb dating of detrital zircons (Zulliger, 2007) established a maximum age of ~97 Ma for the basal quartz rich sandstone (Table 1). The 1,000-m-thick sequence of andesitic volcanoclastic rocks and rhyodacitic tuffs has yielded dates ranging from ~74 to ~64 Ma (Table 1). The older volcanoclastic rocks, which predominate in the northwest sector of the graben, show compositional and age similarities to the Silver King stock, which lies 2 to 4 km northwest of the graben (Fig. 3). The younger quartz-phyric rhyodacite tuffs show a striking resemblance to underlying hypabyssal quartz-phyric rhyodacite Laramide intrusions in the southeast sector of the graben and have similar U-Pb ages (Table 1).

The Resolution graben is bounded by the North, South, and West Boundary faults. The structural and kinematic complexity required to accommodate development of a graben with more than 1 km of displacement along multiple faults was discussed by Manske and Paul (2002). That necessary complexity has since increased with recognition that varying amounts of Paleozoic strata are missing within the graben. Our present interpretation is that the boundary faults originally bounded a horst, the uplift of which facilitated differential erosion of Paleozoic strata. Evidence for erosion as the mechanism for removal of Paleozoic strata includes an irregular unconformable Paleozoic-Cretaceous contact, the normal sequence of lower Paleozoic strata in contact with the underlying Apache Group sedimentary rocks, and the lack of recognizable, low-angle faults other than minor, bedding-parallel shears.

Evidence from recent drilling suggests the graben developed as an asymmetric, structurally controlled basin, and that the West Boundary fault was a growth fault during deposition of the Kvs. Because the North Boundary and South Boundary faults do not show significant displacement beyond the West Boundary fault, they are inferred to be kinematically linked to the West Boundary fault and to have acted as scissor faults, with progressively more displacement to the west.

The Resolution deposit is centrally located within the Resolution graben. It seems likely that the local extensional environment that generated the graben also controlled the emplacement of a body of magma that exsolved the ore fluids responsible for the deposit.

#### *Age of mineralization*

Mineralization-related radiometric ages for Resolution samples show a plausible sequence. The Re-Os dates for molybdenite at ~65 to 64 Ma overlap the youngest U-Pb ages,

~65 to 64 Ma, for the hypabyssal KTrdp intrusions (Table 1). The youngest Re-Os molybdenite age at ~64 Ma is followed by slightly younger  $^{40}\text{Ar}/^{39}\text{Ar}$  ages for secondary biotite and sericite, which range from ~63.5 to ~62 Ma. Four of eight alunite  $^{40}\text{Ar}/^{39}\text{Ar}$  ages are still younger at ~62.3 to ~60.4 Ma. The alunite is paragenetically younger than the biotite and sericite but it is unclear whether the alunite ages reflect cooling rates (Arribas et al., 2011). The decrease in radiometric ages, ~65 to 64 Ma (molybdenite) → ~63.5 to 62 Ma (biotite-sericite) → ~62 to 60 Ma (alunite), presents a consistent pattern that fits the observed paragenetic relationships, and also matches the general trend in closure temperatures for these minerals.

A ~51.4 Ma Re-Os age for pyrite from a massive pyrite-dickite vein together with  $^{40}\text{Ar}/^{39}\text{Ar}$  dates of ~51.7 to 49.4 Ma for two hypogene alunite veins suggests that a younger hydrothermal event may be superimposed on the Resolution system.

#### *Causative intrusion*

The Globe-Miami-Superior mineral belt is centered on the Schultze Granite, a 12-km-long, E-NE elongate multiphase intrusion, the western end of which is shown in Figure 3. The granite exhibits a variety of textures but has a consistent composition, with 70 to 74%  $\text{SiO}_2$ , biotite and quartz phenocrysts, and characteristic megacrysts of orthoclase. U-Pb zircon ages for the granite range from 67 to 61 Ma (Seedorff et al., 2005b; Stavast, 2006). Deep portions of the pluton are well exposed by faulting, uplift, and erosion but show no evidence of underplating or interaction with primitive mafic rocks.

The Schultze Granite is more siliceous than the intrusions associated with most porphyry copper deposits; however, porphyritic phases of the Schultze Granite are intimately related to copper mineralization at the Pinto Valley, Miami-Inspiration, and Copper cities (Peterson, 1954; Stavast, 2006). We cannot explicitly invoke the Schultze Granite as the causative intrusion at Resolution, but some of the hypabyssal intrusions at Resolution show K-feldspar phenocrysts up to 30 mm across, similar to those seen in the Schultze Granite. Neither do we see indications of a distinctly different type of intrusion at Resolution; for example, shoshonitic dikes and mafic rock xenoliths are absent.

Laramide intrusive rocks host only 15% of the material within the 1% Cu Shell (Table 3) and are limited to a swarm of narrow dikes that trend east-west to east-northeast through the center of the deposit, and two small stocks at its margins. Drilling to date has not encountered a stock that is central to the distribution of mineralization and alteration.

Schwarz (2010, fig. 37) demonstrated that the biotite-foliation within potassically altered diabase at Resolution defines a broad dome centered on the eastern portion of the orebody. He suggested that the foliation could have developed at a level below the brittle-ductile transition (Fournier, 1999) in response to local stresses imparted by the intrusion of a hypothetical stock located beneath the deposit at depths below the current drill holes.

#### *Shape of the copper deposit and lack of dismemberment*

The outer limits of the Resolution deposit are not yet well defined but the 1% Cu Shell as presently known takes the form of a thick, approximately upright tortoise shell. The vertical

thickness of the zone of >1% Cu mineralization reaches a maximum of about 600 m in the center of the shell. The steep limbs are incompletely defined because they persist to the bottoms of the deepest drill holes. The geometry and copper distribution seen at Resolution are illustrated in plan and section in Figure 10, where they are compared to the geometries and copper distributions related to the huge porphyry copper deposits at Bingham Canyon, Utah, Hugo Dummett North, Mongolia, and Grasberg, Papua.

Based on the regular boundaries of the mineralized zone and internal mineralization and alteration zoning patterns, the portion of the Resolution deposit explored to date does not appear to be dismembered or even strongly offset by post-mineral faults. Bedding orientations near the base of the post-mineral Whitetail Conglomerate suggest that the Resolution deposit has been rotated to the east-northeast by  $\sim 25^\circ$ . This rotation is assumed to be a consequence of Tertiary displacement on the Devils Canyon and Conley Springs normal faults.

#### *Reason for high hypogene copper grades*

The average copper grade of the Resolution Inferred Resource is 1.47% Cu, which is unusually high for hypogene deposits within the Southwest North America porphyry copper

province (Leveille and Stegen, 2012). One reason for the relatively high grade is the absence of syn- and post-mineral dikes that commonly cause dilution in porphyry deposits. However, other factors play a role, the most important likely being the presence of favorable host rocks. Proterozoic diabase constitutes 36% of the material within the 1% Cu Shell (Table 3) and is an excellent copper host, likely due to its Fe-rich nature (Sillitoe, 2010). Skarns, replacing Proterozoic and Paleozoic carbonates, constitute 10% of the material within the 1% Cu Shell (Table 3) and also host much higher grade than average copper mineralization.

Another important cause of high copper grades at Resolution is that the stage marked by quartz-sericite-pyrite alteration appears to have contributed additional copper as chalcopyrite, bornite, and chalcocite rather than depleting the copper grade as in many other deposits. Hypogene enrichment, due to late-stage replacement of chalcopyrite by bornite, chalcocite, and digenite (Fig. 8), may have also played a role. Bornite and chalcocite are locally the predominant copper sulfides in the portion of the deposit characterized by advanced argillic alteration (Fig. 5F). Examination of the resource model shows that the grade of rhyodacite porphyry within the chalcocite-bornite-dominant domain is 40%

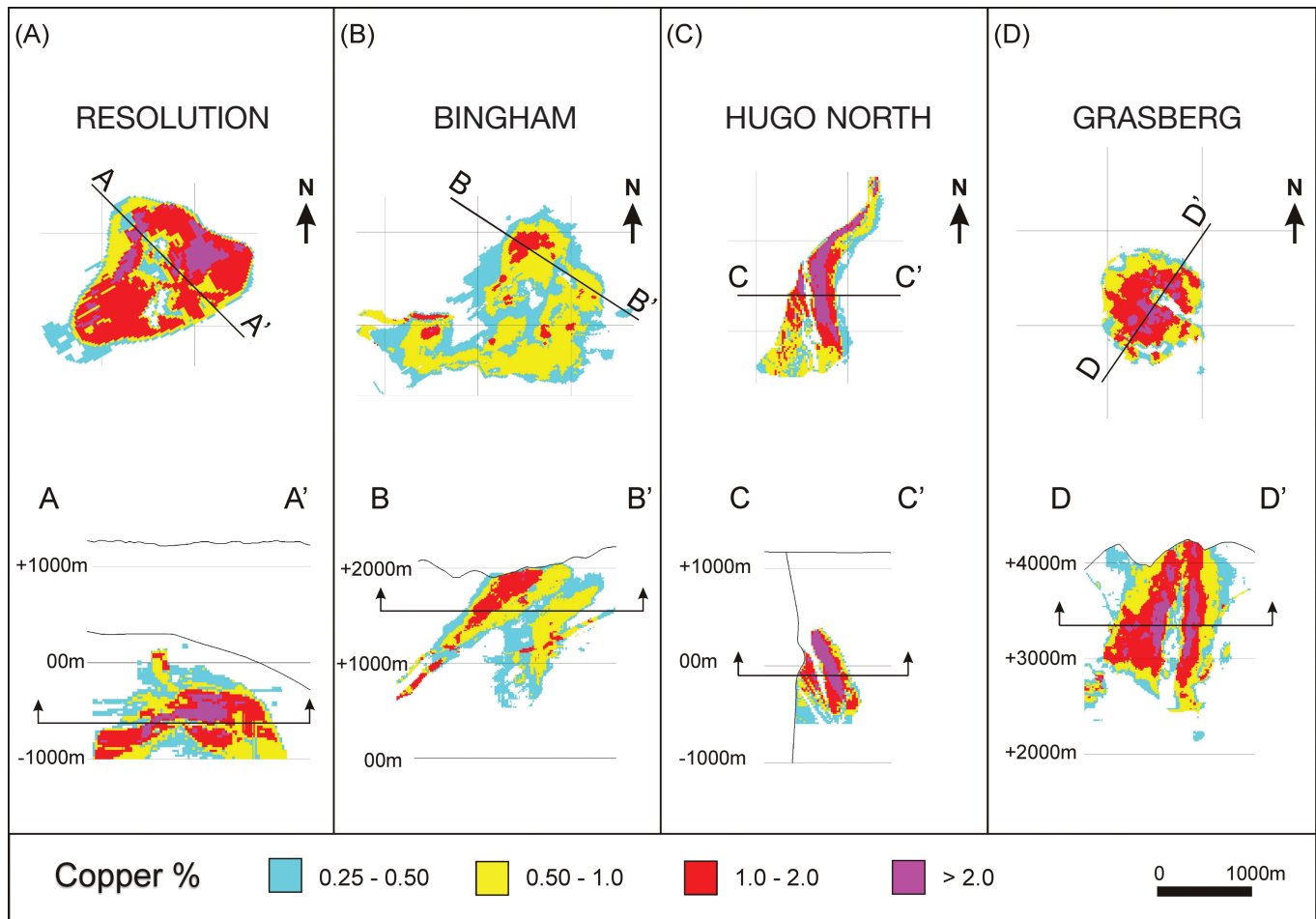


FIG. 10. Level plans and cross sections showing the geometry of Cu grade distribution at the Resolution, Bingham, Hugo Dummett, and Grasberg porphyry copper deposits. The elevation of the plan maps is shown in the sections.

higher on average than the grade of the same lithology within the chalcopyrite-dominant domain (Table 3).

### Conclusions

The Resolution deposit is a deep, high-grade hypogene porphyry Cu-Mo deposit hosted by Proterozoic and Paleozoic quartzite and carbonate units, Proterozoic diabase sills, and Cretaceous sandstones, volcanoclastic rocks, and tuffs. Minor premineral felsic porphyry intrusions host only ~15% of the resource and a centrally located stock that clearly controls the distribution of alteration and mineralization has yet to be defined. U-Pb zircon ages for intrusions in the vicinity of the deposit span ~5 m.y., from ~69 to ~64 Ma, and Re-Os molybdenite ages range from ~65 to ~64 Ma. The deposit is tilted ~25° to the east-northeast and has not been significantly dismembered by Tertiary extension.

High hypogene copper grades in the Resolution deposit resulted from (1) favorable diabase and limestone host rocks, (2) additional chalcopyrite, bornite, and chalcocite mineralization introduced during quartz-sericite-pyrite alteration, and (3) a late stage of mineralization associated with advanced argillic alteration during which earlier chalcopyrite was replaced by bornite, chalcocite, and digenite. High hypogene copper grades may also result from an atypically long period of ore fluid flux focused through centrally located pre- and syn-mineral breccias that provided conduits through subhorizontal diabase sills. Such a sustained flux of hydrothermal fluids may have resulted in deposition of ore several hundred meters above an as-yet unseen intrusion that exsolved the ore fluid.

### Acknowledgments

We appreciate the courtesy that Scott Manske and Don Hammer extended to us as we attempted to understand the geology of the Superior district. We also acknowledge contributions from numerous past and present geologic colleagues at Resolution, including former chief geologists Dave Andrews, Tim Marsh, and Gustavo Zulliger. We especially acknowledge the contributions of Gustavo whose persistent observations led to a preliminary stratigraphy for the Cretaceous sedimentary and volcanic units. Marco Einaudi, Lewis Gustafson, William Chavez, John Proffett, Eric Seedorff, and Richard Sillitoe are thanked for helpful suggestions and insights. We thank Rio Tinto and BHP Billiton for permission to publish, Michael Alvarez for drawing the figures, Jay Hammitt for a review of an early draft, and Scott Manske and Gustavo Zulliger for reviews on behalf of the editors.

### REFERENCES

- Arribas, A., Arribas, I., Draper, G., Hall, C., Kesler, S.E., McEwan, C., and Muntean, J.L., 2011, <sup>40</sup>Ar/<sup>39</sup>Ar Dating of alunite from the Pueblo Viejo gold-silver district, Dominican Republic, *Economic Geology*, v. 106, p. 1059–1070.
- Ballantyne, G. H., Marsh, T. M., Hehnke, C., Andrews, D. S., Eichenlaub, A. B., and Krahulec, K. A., 2003, The Resolution copper deposit, a deep, high-grade porphyry copper deposit in the Superior district, Arizona: Marcofest Conference, Golden, Colorado, 3–5 April 2003, Society of Economic Geologists Student Chapter, Colorado School of Mines, CD Publication, 12 p.
- BHP Billiton, 2009, Annual Report.
- Chappell, G., 1973, Rails to carry copper: Boulder, Colorado, Pruett Publishing, 255 p.
- Cornwall, H.R., Banks, N.G., and Phillips, C.H., 1971, Geologic map of the Sonora quadrangle, Pinal and Gila counties, Arizona: U.S. Geological Survey quadrangle map GQ-1021, 1:24,000.
- Creasey, S.C., 1980, Chronology of intrusion and deposition of porphyry copper ores, Globe-Miami district, Arizona: *Economic Geology*, v. 75, p. 830–844.
- Creasey, S.C., Peterson, D.W., and Gambell, N.A., 1983, Geologic map of the Teapot Mountain quadrangle, Pinal County, Arizona: U.S. Geological Survey quadrangle map GQ-1559, 1:24,000.
- Einaudi, M.T., 1982, Description of skams associated with porphyry copper plutons, in Titley, S.R., ed., *Advances in geology of the porphyry copper deposits, southwestern North America*: Tucson, Arizona, University of Arizona Press, p. 139–184.
- Ferguson, C.A., Skotnicki, S.J., and McIntosh, W.C., 1998, Rapid extensional tectonism and short-lived volcanism along the Transition zone, Basin and Range boundary, central Arizona [abs.]: *Geological Society of America Abstracts with Programs*, v. 30, no. 6, p. 9.
- Ford, J.D., 1978, A chemical study of alteration at the Panguna porphyry copper deposit, Bougainville, Papua New Guinea: *Economic Geology*, v. 73, p. 703–720.
- Fournier, R.O., 1999, Hydrothermal processes related to movement of fluid from plastic into brittle rock in the magmatic-epithermal environment: *Economic Geology*, v. 94, p. 1193–1211.
- Grupo Mexico, 2010, Annual Report.
- Gustafson, L.B., and Hunt, J.P., 1975, The porphyry copper deposit at El Salvador, Chile: *Economic Geology*, v. 70, p. 857–912.
- Hammer, D.F., 1967, Structural nature of the Magma “Breccia”: Unpublished internal report to Magma Copper Co., 10 p.
- 1972, Geologic investigation of the Superior area, Pinal county, Arizona: Unpublished Newmont Exploration Ltd. report to Magma Copper Co., 56 p. plus appendices.
- 1989, Potential for discovery of additional ore in the Magma mine: Unpublished report to Magma Copper Co., 52 p.
- Hammer, D.H., and Peterson, D.W., 1968, Geology of the Magma mine area, Arizona, in Ridge, J.D., ed., *Ore deposits in the United States*, (Graton-Sales Volume): New York, American Institute of Mining, Metallurgical, and Petroleum Engineers, v. 2, p. 1282–1310.
- Harrison, R., 2007, The evolution of hydrothermal alteration—mineralisation events in the Resolution Cu-Mo deposit, Superior, Arizona: Unpublished M.Sc. thesis, Bristol, England, University of Bristol, 43 p.
- Heidrick, T.L., and Titley, S.R., 1982, Fracture and dike patterns in Laramide plutons and their structural and tectonic implications, in Titley, S.R., ed., *Advances in geology of the porphyry copper deposits, southwestern United States*: Tucson, University of Arizona Press, p. 73–92.
- Keep, M., 1996, The Pinal Schist, southeast Arizona, USA—contraction of a Palaeoproterozoic rift basin: *Journal of the Geological Society, London*, v. 153, p. 979–993.
- Keith, S.B., 1986, A contribution to the geology and tectonics of the Ray-Superior region, Pinal county, Arizona: *Arizona Geological Society Digest*, v. 16, p. 392–407.
- Keith, S.B., and Swan, M.M., 1995, Tectonic setting, petrology, and genesis of the Laramide porphyry copper cluster of Arizona, Sonora, and New Mexico: *Arizona Geological Society Digest*, v. 20, p. 339–346.
- Leveille, R.A., and Stegen, R.J., 2012, The southwestern North America porphyry copper province: *Society of Economic Geologists Special Publication* 16, p. 361–401.
- Lowell, J.D., and Guilbert, J.M., 1970, Lateral and vertical alteration-mineralization zoning in porphyry deposits: *Economic Geology*, v. 65, p. 373–408.
- Maher, D.J., 2008, Reconstruction of Middle Tertiary extension and Laramide porphyry copper systems, east-central Arizona: Unpublished Ph.D. dissertation, Tucson, AZ, University of Arizona, 328 p.
- Manske, S.L., and Paul, A.H., 2002, Geology of a major new porphyry copper center in the Superior (Pioneer) district, Arizona: *Economic Geology*, v. 97, p. 197–220.
- Paul, A.H., and Knight, M.J., 1995, Replacement ores in the Magma mine, Superior, Arizona: *Arizona Geological Society Digest*, v. 20, p. 366–372.
- Paul, A.H., and Manske, S.L., 1998, History of exploration at the Magma mine, Superior, Arizona: Unpublished internal report to BHP, 29 p.
- Perry, D.V., 1969, Skam genesis at the Christmas mine, Gila Co., Arizona: *Economic Geology*, v. 64, p. 255–270.
- Peterson, D.W., 1961, Dacitic ash-flow sheet near Superior and Globe, Arizona: Unpublished Ph.D. thesis, Stanford, CA, Stanford University, 130 p.; published as U.S. Geological Survey Open-File Report, April 3, 1961, 130 p.
- Peterson, D.W., 1969, Geologic map of the Superior quadrangle, Pinal county, Arizona: U.S. Geological Survey quadrangle map GQ-818, 1:24,000.

- Peterson, N.P., 1954, Copper Cities copper deposit, Globe-Miami district, Arizona: *Economic Geology*, v. 49, p. 362–377.
- 1962, Geology and ore deposits of the Globe-Miami district, Arizona: U.S. Geological Survey Professional Paper 342, p. 151.
- 1963, Geology of the Pinal Ranch quadrangle, Arizona: U.S. Geological Survey Bulletin 1141-H, 18 p.
- Phillips, C.H., Gambell, N.A., and Fountain, D.S., 1974, Hydrothermal alteration, mineralization, and zoning in the Ray deposit: *Economic Geology*, v. 69, p. 1237–1250.
- Ransome, F.L., 1912, Copper deposits near Superior, Arizona: U.S. Geological Survey Bulletin 540, p. 139–158.
- Richard, S.M., and Spencer, J.E., 1998, Compilation geologic map of the Ray-Superior area, central Arizona: Arizona Geological Survey Open-File Report 98-13.
- Rio Tinto, 2010, Annual Report.
- Schott, T.G., 1994, Mineralization, lithology, and alteration in the Mesozoic rocks, Superior mine (sic), Superior, Arizona: Unpublished M.Sc. thesis, Socorro, New Mexico, New Mexico Institute of Mining and Technology, 197 p.
- Schwarz, A.C., 2010, Early diabase-hosted alteration mineralization in the Resolution Cu-Mo deposit, Pinal county, Arizona: the foundation of a giant porphyry system: Unpublished M.Sc. thesis, Canada, Queen's University, 144 p.
- Seedorff, E., Dilles, J.H., Proffett, J.M., Jr., Einaudi, M.T., Zurcher, L., William J. A. Stavast, W. J.A., Johnson, D.A., Barton, M.D., 2005a, Porphyry-related deposits: Characteristics and origin of hypogene features: *Economic Geology 100<sup>th</sup> Anniversary Volume*, p. 251–298.
- Seedorff, E., Barton, M.D., Gehrels, G.E., Johnson, D.A., Maher, D.J., Stavast, W.J.A., and Flesch, E., 2005b, Implications of new U-Pb dates from porphyry copper related plutons in the Superior-Globe-Ray-Christmas area, Arizona [abs.]: *Geological Society of America Abstracts with Programs*, v. 37, no. 7, p. 164.
- Sell, J.D., 1995, Discovery of a deep (3500 feet) unexposed porphyry copper deposit at Superior East, Pinal county, Arizona: *Arizona Geological Society Digest*, v. 20, p. 373–395.
- Short, M.N., Galbraith, F.W., Harshman, E.N., Kuhn, T.H., and Wilson, E.D., 1943, Geology and ore deposits of the Superior mining area, Arizona: Arizona Bureau of Mines, Geological Series 16, Bulletin 51, 159 p.
- Sillitoe, R.H., 2010, Porphyry copper systems: *Economic Geology*, v. 105, p. 3–41.
- Singer, D.A., Berger, V.I., and Moring, B.C., 2008, Porphyry copper deposits of the world—database and grade and tonnage models, 2008: U.S. Geological Survey Open-File Report 2008–1155, 45 p., <http://pubs.usgs.gov/of/2008/1155/>.
- Stavast, W.J.A., 2006, Three-dimensional evolution of magmatic hydrothermal systems, Schultze Granite and Ruby Star Granodiorite, Arizona: Unpublished Ph.D. dissertation, Tucson, AZ, University of Arizona, 414 p.
- Stein, H.J., Morgan, J.W., and Scherstén, A., 2000, Re-Os dating of low-level highly radiogenic (LLHR) sulfides: the Harnäs gold deposit, southwest Sweden records continental scale tectonic events: *Economic Geology*, v. 95, p. 1657–1671.
- Stein, H.J., Markey, R.J., Morgan, J.W., Hannah, J.L., and Scherstén, A., 2001, The remarkable Re-Os chronometer in molybdenite: How and why it works: *Terra Nova*, v. 13, p. 479–486.
- Titely, S.R., 1982, Geologic setting of porphyry copper deposits, in Titely, S.R., ed., *Advances in geology of the porphyry copper deposits, southwestern North America*: Tucson, University of Arizona Press, p. 93–116.
- Troutman, S.M., 2001, Advanced argillic alteration in the deeply buried Magma porphyry Cu-Mo prospect, Superior, Arizona: Unpublished M.Sc. thesis, Stanford, CA, Stanford University, 115 p.
- U.S. Geological Survey, 2002, Magnetic anomaly map of North America, online at: [http://pubs.usgs.gov/sm/mag\\_map/mag\\_s.pdf](http://pubs.usgs.gov/sm/mag_map/mag_s.pdf).
- Winant, A.R., 2010, Sericitic and advanced argillic mineral assemblages and their relationship to copper mineralization, Resolution porphyry Cu-(Mo) deposit, Superior district, Pinal County, Arizona: Unpublished M.Sc. thesis, Tucson, AZ, University of Arizona, 79 p.
- Wrucke, C.T., 1989, The Middle Proterozoic Apache Group, Troy Quartzite, and associated diabase of Arizona: *Arizona Geological Society Digest* v. 17, p. 239–258.
- Zimmerman, A., Stein, H.J., Hannah, J.L., Kozelj, D., Bogdanov, K., and Berza, T., 2008, Tectonic configuration of the Apusini-Banat-Timok-Srednogie belt, Balkans-South Carpathians, constrained by high precision Re-Os molybdenite ages: *Mineralium Deposita*, v. 43, p. 1–21.
- Zulliger, G.A., 2007, Mid-late Cretaceous stratigraphy and volcanic-intrusive transition at the Resolution porphyry Cu-Mo deposit, SW Arizona: Age and timing constraints based on U/Pb, Re/Os and <sup>40</sup>Ar/<sup>39</sup>Ar dating: Internal report to Resolution Copper Mining L.L.C., 41 p.